

DEVELOPMENT OF A CYCLOIDAL PROPULSION COMPUTER MODEL AND  
COMPARISON WITH EXPERIMENT

By

Michael Lynn McNabb

A Thesis  
Submitted to the Faculty of  
Mississippi State University  
in Partial Fulfillment of the Requirements  
for the Degree of Master of Science  
in Engineering  
in the Department of Aerospace Engineering

Mississippi State, Mississippi

December 2001

Name: Michael Lynn McNabb

Date of Degree: December 14, 2001

Institution: Mississippi State University

Major Field: Aerospace Engineering

Major Professor: Dr. George Bennett

Title of Study: DEVELOPMENT OF A CYCLOIDAL PROPULSION COMPUTER  
MODEL AND COMPARISON WITH EXPERIMENT

Pages in Study: 68

Candidate for Degree of Masters of Science

Simplified unsteady aerodynamic and inertial force models were developed for a cycloidal propeller system operating at small forward speeds. These models were used to support the development of a VTOL concept demonstrator vehicle. The nature of the blade motion showed that interactions between the blades could be neglected to first order. The downwash through the rotor could not be neglected because of the induced angle of attack caused by the downwash.

The total force produced by the propeller was compared with wind tunnel data produced by Wheatley in the 30's and a ground test system developed for this project. It was found that the estimates produced by the model agreed with the total force and power to within 10% for the Wheatley data. Agreement between the model and the current tests was within 5% for the total force and power.

The calculated inertial loads were used to design the blade structure, the support structure, and the blade motion control system. It was found that the inertial loads were much larger than the aerodynamic loads.

The aerodynamic effect of forward motion or wind moving toward the propeller was defined. It was modeled as a constant velocity induced flow through the propeller that induced an angle of attack of the blades. It was found that the cycloidal propeller was very susceptible to wind gusts, but that the resultant force from the wind gust could be easily damped out.

The same forward motion model was used to simulate downwash. By modeling the downwash as a constant velocity flow through the propeller, the lift and thrust of the propeller was linked to the induced flow velocity. The effect of the induced flow velocity was then linked back to its effect on the lift and thrust produced by the propeller.

## ACKNOWLEDGEMENTS

I would like to thank my loving wife for her patience, persistent nagging to finish my schoolwork, and support during my eight years at Mississippi State University.

I would like to thank the now retired Dr. George Bennett for his guidance in the last five years while working at Raspet Flight Lab and during my thesis work. I would also like to thank the department of Aerospace Engineering at Mississippi State for being such good teachers of the art of work and life, as well as the entire university for teaching me what it is to be a Bulldog.

# TABLE OF CONTENTS

	Page
ACKNOWLEDGEMENTS .....	iii
TABLE OF CONTENTS .....	iv
LIST OF TABLES .....	vi
LIST OF FIGURES.....	vii
LIST OF SYMBOLS AND ABBREVIATIONS .....	ix
 CHAPTER	
I. INTRODUCTION .....	1
CYCLOIDAL PROPELLER HISTORY .....	1
BACKGROUND .....	1
THE COORDINATE SYSTEM.....	3
VARIABLES FOR THE CYCLOIDAL PROPELLER .....	4
Airfoil .....	4
Diameter .....	4
Span .....	4
Number of Blades .....	5
Chord .....	6
Speed of Rotation.....	6
METHOD OF CALCULATION .....	6
II. METHODS OF MODELING.....	7
IDEAL MOTION WITH STEADY AERODYNAMICS.....	7
IDEAL MOTION WITH UNSTEADY AERODYNAMICS .....	10
REAL MOTION WITH UNSTEADY AERODYNAMICS.....	15
III. DYNAMIC EFFECTS.....	19
FORWARD MOTION.....	19
DOWNWASH.....	21
WIND GUSTS.....	22
FORWARD MOTION BY ROTATING PHI.....	22
CAM SHAPES REQUIRED FOR FORWARD MOTION.....	23
IV. COMPARISON OF COMPUTER MODEL WITH WHEATLEY WIND TUNNEL DATA.....	25
V. COMPARISON OF MODEL WITH EXPERIMENT.....	27
CYCLOIDAL PROPELLER DESIGNED FOR BOSCH AEROSPACE .....	27
Airfoil .....	27
Diameter .....	27

CHAPTER	Page
Span .....	28
Number of Blades .....	28
Chord .....	28
Speed of Rotation.....	28
COMPARISON OF DIFFERENT COMPUTER MODELS.....	28
TESTING HISTORY.....	32
Test Rig.....	32
Blades .....	33
Push-Pull Rods.....	35
COMPARISON OF THE COMPUTER MODEL AND TEST DATA .....	35
VI. CONCLUSIONS.....	37
BIBLIOGRAPHY .....	39
APPENDIX	
A. FIGURES.....	40
B. MATHCAD PREGRAM.....	58
C. REAL MOTION UNSTEADY AERODYNAMICS PROGRAM .....	61

## LIST OF TABLES

TABLE	Page
1. DERIVATION OF INDUCED AOA EQUATION.....	20
2. MAGNITUDE OF BLADE FORCE IN X DIRECTION.....	31
3. PROGRAM OUTPUT THAT IS NOT A FUNCTION OF THETA .....	32

## LIST OF FIGURES

FIGURE	Page
A1. CANTILEVERED CYCLOIDAL PROPELLER.....	41
A2. COMMANDED BLADE ANGLE.....	41
A3. COORDINATE SYSTEM .....	42
A4. EFFECT OF THE NUMBER OF BLADES. ....	42
A5. LIFT AND DRAG .....	43
A6. DEFINITION OF VARIABLES IN UNSTEADY AERODYNAMICS EQUATIONS .....	43
A7. PLOT OF F AND G.....	43
A8. FOUR-BAR LINKAGE CONTROL MECHANISM .....	44
A9. COMPARISON OF IDEAL MOTION AND REAL MOTION.....	44
A10. TYPICAL FOUR-BAR SYSTEM.....	45
A11. DEFINITION OF PROPELLER MOTION.....	45
A12. RETARDING FORCE/DRAG DUE TO GUST .....	46
A13. INCREASE IN LIFT DUE TO GUST .....	46
A14. INCREASE IN HP DUE TO GUST .....	47
A15. COMMANDED PHI NEEDED FOR FORWARD FLIGHT .....	47
A16. OFFSET REQUIRED FOR DIFFERENT FORWARD SPEEDS.....	48
A17. HP REQUIRED FOR DIFFERENT FORWARD SPEEDS .....	48
A18. CAM SHAPE NEEDED FOR ADVANCE RATIOS EQUAL TO 0.5 AND 1.5 .....	49
A19. CAM SHAPE NEEDED FOR ALL ADVANCE RATIOS BETWEEN 0.0 AND 2.0 .....	49
A20. COMPARISON TO WHEATLEY'S WIND TUNNEL DATA FOR FORCE IN Z DIRECTION .....	50
A21. COMPARISON TO WHEATLEY'S WIND TUNNEL DATA FOR FORCE IN X DIRECTION .....	50
A22. COMPARISON TO WHEATLEY'S WIND TUNNEL DATA FOR POWER.....	51
A23. COMPARING WHEATLEY'S AND THE PROGRAM'S DATA FOR DIFFERENT FORWARD SPEEDS.....	51

FIGURE	Page
A24. ANGULAR VELOCITY OF THE BLADE .....	52
A25. ANGULAR ACCELERATION OF THE BLADE.....	52
A26. INDUCED AoA CAUSED BY DOWNWASH .....	53
A27. TOTAL AoA OF THE BLADE .....	53
A28. LIFT OF THE BLADE .....	54
A29. DRAG OF THE BLADE .....	54
A30. FORCE IN THE Z DIRECTION PRODUCED BY THE BLADE.....	55
A31. FORCE IN THE X DIRECTION PRODUCED BY THE BLADE .....	55
A32. SKETCH OF TEST RIG .....	56
A33. 3D VIEW OF TEST RIG .....	56
A34. BLADE MEASUREMENTS USED IN BOSCH CYCLOIDAL PROPELLER .....	56
A35. LIFT GENERATED BY CYCLOIDAL PROPELLER COMPARED TO COMPUTER PREDICTIONS .....	57
A36. HP REQUIRED BY CYCLOIDAL PROPELLER COMPARED TO COMPUTER PREDICTIONS .....	57

## LIST OF SYMBOLS AND ABBREVIATIONS

$\alpha, A_oA$	Angle of attack of the blade = $\beta + A_oAW$
$\beta$	Commanded blade angle
$\beta_{max}$	Amplitude of the commanded blade angle
$A_oAW$	Angle of attack induced by the wind
$\theta$	Blade position around the circumference of the circle measured from the X-axis counterclockwise.
$\phi$	Rotation of the Force Vector
$\Omega$	Cycloidal propeller's rotational speed
$\omega$	Blades rotational speed around the pivot point
acc	Blades rotational acceleration around the pivot point
$V_t$	Tangential velocity of the blades = $R * \Omega$
$C_{l\alpha}$	2-D lift curve slope of the airfoil
$C_{L\alpha}$	3-D lift curve slope of the blade
$C_L$	Lift coefficient of the blade
$C_D$	Drag coefficient of the blade and hub arms
$C_{D0}$	Parasite drag coefficient - Zero lift drag coefficient
AR	Aspect ratio of the blade
Eff	Oswald efficiency factor of the blade
$P_d$	The distance from the pivot point to the push-pull rod

$F_x$	Force produced by the propeller in the positive X direction
$F_y$	Force produced by the propeller in the positive Z direction
$V_x$	The velocity of the forward motion of the propeller in the positive X direction, or the velocity of the wind gust in negative X direction.
$V_z$	The velocity of the forward motion of the propeller in the positive Z direction, or the velocity of the wind gust in negative Z direction.
$V_{\text{tangent}}$	The tangential velocity of the wind at the blades due to the rotation and the contributions of $V_x$ and $V_z$
$V_{\text{normal}}$	The normal velocity of the wind at the blades due to the rotation and the contributions of $V_x$ and $V_z$
$V_r$	The resultant velocity of the wind at the blades due to the rotation and the contributions of $V_x$ and $V_z$
b	Semi chord used by the I.E. Garick unsteady lift and pitching moment equations
a	Pivot point measured from the semi chord point aft, used in the I.E. Garick unsteady lift and pitching moment equations
F&G	Attenuation factors used in the I.E. Garick unsteady lift and pitching moment equations
$\kappa$	Reduced frequency of blade oscillation
$a_n$	Normal acceleration on the blades at operating RPM
k	Advance ratio of the cycloidal propeller = $V_{\text{tip}}/V_{\text{forward}}$

# CHAPTER I

## INTRODUCTION

### Cycloidal Propeller History

In the 1920's, a gentleman named Frederick Kurt Kirsten first seriously investigated cycloidal propulsion <sup>(1)</sup>. While working at the University of Washington, Kirsten developed a Pi pitch cycloidal blade motion cycloidal propeller and investigated the possibilities of putting the device on several different air vehicles. In the 1930's Kirsten proposed modifying the U.S. Navy's Shenandoah lighter than airship to use cycloidal propellers, but the Shenandoah crashed before the modification could be made. Also in the 1930's, John B. Wheatley began work on cycloidal propulsion <sup>(2)</sup>. He developed a curate blade motion and developed a supporting modeling theory. Wind tunnel tests at the Langley 20-foot wind tunnel were completed using an 8-foot diameter model. This is the blade motion that will be used for the cycloidal propeller discussed in this thesis.

### Background

A cycloidal propeller is a propeller with the blades parallel to the axis of rotation and perpendicular to the plane of rotation. Figure 1 shows an isometric view of a cycloidal propeller. As the propeller rotates, the blades of the propeller pivot to give an

angle of attack (AoA or  $\alpha$ ), and this is called the commanded blade angle ( $\beta$ ). The commanded blade angle is shown in figure 2. In a hover with no wind gusts, the commanded blade angle is equal to the AoA of the blades. By timing when and where the blades have their maximum and minimum AoA, a force can be produced in any direction in the plane of rotation. This allows a cycloidal propeller to produce lift and thrust at the same time.

The control mechanism developed for the cycloidal propeller is based on a four-bar linkage system controlling the individual blades AoA. This system has the advantage of rugged simplicity while still closely matching the assumed ideal blade AoA profile. By moving a single point common to each of the blades four-bar linkages, the magnitude and direction of the blades AoA profile can be controlled.

The uses of a cycloidal propeller vary widely. The company for which this work was performed, Bosch Aerospace of Huntsville, Al, is using it to develop a Vertical Take Off and Landing Unmanned Aerial Vehicle, (VTOL UAV), with at least two main cycloidal propellers for lift and thrust. This vehicle will weigh 600 lbs. For a factor of safety and to have some maneuvering power, each propeller is designed to produce 350 lbs of lift. Bosch also wants to use cycloidal propulsion on airships, which are difficult to land partly because of the slow response of the rotating ducted fans. This system would make ground control of airships easier. This system is also used on tugboats, for the same reason; a tugboat, like an airship, needs fast response times, and cycloidal propulsion has been shown to be one solution.

In this thesis, the cycloidal propeller computer modeling will be discussed, starting with the coordinate system used, the variables used in the modeling, and

methodology of the calculations. Three of the simplified models developed will also be discussed starting with the simplest, the Ideal motion with Steady Aerodynamics, and ending with the most advanced, the Real Motion with Unsteady Aerodynamics. There is also a discussion of the aerodynamics of the propeller in forward motion. Using the forward motion model, a uniform velocity downwash model was developed. Finally, there is a comparison between the computer model and Wheatly's wind tunnel data, and data taken from the cycloidal propeller built by Bosch Aerospace.

### The coordinate system

The coordinate system that will be used can be seen below as figure 3. The X-axis to the left, the Y-axis is coming out of the picture, and the Z-axis is going up. This coordinate system is different from the coordinate system seen in many aerospace texts. The textbooks typically put the Y-axis on the right wing, making the Z-axis point down. By rotating the coordinate system until the Y-axis points out the left wing, the Z-axis points up. The angle theta ( $\theta$ ) is the position of the blade measured from the X-axis counterclockwise. The angle phi ( $\phi$ ) is the angle from the X-axis to the theta where the AoA is zero, measured counterclockwise. This essentially rotates the lift vector and gives a force in the X and Z directions, or lift and thrust.

## Variables for the Cycloidal Propeller

A cycloidal propeller can be broken down into six variables.

1. The airfoil section
2. The diameter of the propeller
3. The span of the blades
4. The chord of the blades
5. The number of blades
6.  $\Omega$  - The speed of rotation of the propeller

Each of these are described as follows:

### **Airfoil**

The blades have to perform equally well at positive and negative AoA's. This requires the use of a symmetric airfoil, which should have a robust lift curve slope, since this will determine the effectiveness of the propeller. It would be also be beneficial to have an airfoil that has good unsteady aerodynamics characteristics.

### **Diameter**

In general, the larger the diameter of the cycloidal propeller, the better. If tip speed is held constant, larger diameters mean lower rotational speeds, hence lower centrifugal force on the blades.

### **Span**

A paper by Fredric Kurt Kirsten <sup>(1)</sup>, asserts that “The best proportions would be a blade length equal to the orbit diameter, thus providing for maximum slipstream area with minimum dead air envelope.” Simplified, he is suggesting that the span be equal to the diameter.

## **Number of Blades**

It was also mentioned by Kirsten <sup>(1)</sup> and later shown by computer modeling that a cycloidal propeller with less than four blades is noticeably bumpy. This occurs because only one or two blades are producing lift at any one time. A cycloidal propeller with two blades can produce lift only when the blades are in the theta equals  $90^\circ$  or  $270^\circ$  position. At all other thetas, the blades are producing only limited force. This results in a very bumpy ride with the frequency of the “bumps” equal to twice the rotational speed.

With three blades, the ride is improved, because there is not a big impulse at theta equals  $90^\circ/270^\circ$ , and the vibration frequency is three times the rotational speed. However, there is still only one blade producing force at any one point. This means that the entire required lift must be generated by only one blade. This in turn requires a heavier blade.

With four or more blades, there is always more than one blade producing lift. The vibration frequency is increased to four times the rotational speed, with the lift peaks occurring at  $0^\circ/180^\circ$  and  $90^\circ/270^\circ$ .

A six-bladed propeller gives the advantage of a vibration frequency of six times the rotational speed, and allows more than one blade to produce the required instantaneous lift, which smoothes out the system considerably. The comparison between a four-bladed helicopter and a two-bladed helicopter illustrates this point. A four or six-bladed helicopter is often much smoother than the two bladed Huey.

A plot of the lift force produced by a two, three, four, and six bladed cycloidal propeller can be seen in figure 4 in the appendix.

### **Chord**

The further apart the blades, the cleaner the air encountered by the blade.

The chord needs to be as large as possible to produce as much force as possible.

This is difficult within a small diameter propeller.

### **Speed of Rotation**

In general, the slower the propeller turns, the better. This is due to the centrifugal load on the blades. Since the diameter is set, the required “ $q$ ”, or dynamic pressure over the blades must still be generated. Given logical choices for all the previous variables, the rotational speed of the propeller can be adjusted to give the required lift and thrust force from the propeller.

### **Method of Calculation**

To calculate the total lift and drag of the propeller, first determine the individual blade position. Given the position of the blade, the AoA of the blade can be calculated. With the blades position and AoA known the lift, drag, and pitching moment of the blades can be found. The resultant forces from each blade in the X and Z directions can then be summed. After calculating the resultant forces, the entire propeller can be rotated to give a new blade position, AoA, lift, drag, and pitching moment.

## CHAPTER II

### METHODS OF MODELING

#### Ideal Motion with Steady Aerodynamics

From early inspection of the nature of a cycloidal propeller, it is apparent that the ideal blade motion for a hovering cycloidal propeller is a sinusoidal motion, where the blade “takes a bite” at the top and at the bottom. In a hover, the propeller is required to produce lift in the positive Z direction. To do this, the blades should have a negative AoA at the bottom, theta equals 90°, and a positive AoA at the top, theta equals 270°. The motion of the blades can be described as a negative sine motion. In a hover, the commanded blade angle  $\beta$  is equal to the AoA of the blades, which also makes  $\beta$  a negative sine motion. The angle  $\phi$  rotates the place where the zero AoA is located. When theta equals phi, the AoA should be zero. The equation for the commanded blade angle can be seen below.

$$\beta = -\beta_{Max} * \sin(\theta - \phi) \quad \text{Equation 1}$$

where  $\beta_{Max}$  is the amplitude of the sine motion. Given that the AoA of the blade is defined, the next step is to calculate the lift curve slope of the NACA 0012. To calculate the 3-D lift curve slope,  $C_{L\alpha}$ , the 2-D lift curve slope,  $C_{l\alpha}$  must be known.  $C_{l\alpha}$  is found experimentally using wind tunnels, and is based on an infinite wing where the airfoil does not see any effects from the tip of the airfoil. Given the  $C_{l\alpha}$  for a NACA 0012 is 6.0161<sup>(3)</sup>

the next step is to determine the 3-D lift curve slope of the blade,  $C_{L\alpha}$ . The equation for  $C_{L\alpha}$  given by Etkin<sup>(4)</sup> is listed below.

$$C_{L\alpha} = \frac{2 * \pi * AR}{2 + \sqrt{\frac{AR^2 * \beta^2}{\kappa^2} + \frac{\tan^2(\Lambda/2)}{\beta^2} + 4}} \quad \kappa = \frac{\beta * C_{l\alpha}}{2 * \pi} \quad \beta = \sqrt{1 - Mach} \quad \text{Equation 2}$$

where AR is the aspect ratio of the blades. Equation 2 can be simplified for the propeller being discussed in this thesis. The tip speed of the propeller is 136 ft/s, which is much less than the speed of sound. This means that the variable  $\beta$  is approximately equal to 1. The blades do not have any sweep, so  $\Lambda = 0$ . This simplifies equation 2 to the following equation.

$$C_{L\alpha 3-D} = \frac{2 * \pi * AR}{2 + \sqrt{\frac{AR^2 * 4 * \pi^2}{C_{l\alpha}^2} + 4}} \quad \text{Equation 3}$$

Since the AoA of the blade and the lift curve slope of the blade are both known, the lift coefficient for the blade at that theta can be found using the following equation.

$$C_L = C_{L\alpha 3-D} * \alpha \quad \text{Equation 4}$$

Once the lift coefficient is known, the lift can be found using the standard lift equation seen below.

$$Lift = \frac{1}{2} * \rho * V^2 * S * C_L = \frac{1}{2} * \rho * V_t^2 * (Span * Chord) * C_L \quad \text{Equation 5}$$

where  $V_t$  is the tip speed of the propeller in ft/second and is equal to  $\Omega * R$ . In this section, it is assumed that the only drag associated with the blade is the induced drag, because at the time of the analysis the cycloidal propeller was a ‘paper model’ used as a

sizing routine. To calculate the induced drag of the blade, the drag coefficient must be found using the drag polar. The equation for the drag polar can be seen below.

$$C_D = C_{D0} + \frac{C_L^2}{\pi * AR * Eff} \quad \text{Equation 6}$$

where Eff is the Oswald span efficiency factor. This is a “fudge factor” and will be used to match the computed data to experimental data. Once the drag coefficient is known, the drag can be computed using the following equation.

$$Drag = \frac{1}{2} * \rho * V^2 * S * C_D = \frac{1}{2} * \rho * V_t^2 * (Span * Chord) * C_D \quad \text{Equation 7}$$

The next step is to resolve the lift and drag forces into forces into the X and Z coordinate system. Figure 5 shows the blades lift and drag vector at four different thetas. To transform the lift and drag produced by the blades into forces in the X and Z directions a coordinate transformation, which transforms from a rotating coordinate system, rotating about the Y-axis, to the stationary coordinate system. The coordinate transformation can be seen below as equation 8.

$$\begin{aligned} i_{Fixed} &= i_{Rotating} * \cos(\varphi) + k_{Rotating} * \sin(\varphi) \\ j_{Fixed} &= j_{Rotating} \\ k_{Fixed} &= -i_{Rotating} * \sin(\varphi) + k_{Rotating} * \cos(\varphi) \end{aligned} \quad \text{Equation 8}$$

where  $\varphi$  is the angle between the two coordinate systems. The angle  $\varphi$  is equivalent to theta, the total propeller's thrust,  $F_x$ , is in the 'i<sub>Fixed</sub>' direction, the total propeller's lift,  $F_z$ , is in the 'k<sub>Fixed</sub>' direction, the blade's lift is in the 'i<sub>Rotating</sub>' direction, and the blade's drag is in the 'k<sub>Rotating</sub>' direction. Substituting into equation 8 for the force in the X direction, the equation for the force in the X direction becomes the following:

$$F_x = Lift * \cos(\theta) + Drag * \sin(\theta) \quad \text{Equation 9}$$

Substituting into equation 8 for the force in the Z direction, the equation for the force in the Z direction becomes the following:

$$F_z = -Lift * \sin(\theta) + Drag * \cos(\theta) \quad \text{Equation 10}$$

Since the force in the X and Z directions are known for a blade at a theta, the total force can be determined. To determine the average force produced by the cycloidal propeller, all the  $F_x$ , and  $F_z$  produced by all the blades over all thetas are summed. The torque and power required to turn the propeller can be approximated by the following equations.

$$Torque = \sum_{\theta=0}^{360} \sum_{\text{Number of blades}} Drag * Radius \quad \text{Equation 11}$$

$$Power = \sum_{\theta=0}^{360} \sum_{\text{Number of blades}} \frac{Drag * V_t}{550}$$

Appendix 1 contains a MathCad sheet that illustrates the above steps. Appendix 1 is included to show that the FORTRAN program operates correctly and that the steps are laid out in logical order. The MathCad sheet starts with the geometric properties of the cycloidal propeller, calculates the velocity the blades, the lift and drag of the blades, and the forces in the X and the Z direction. Then it averages them over one full rotation.

### Ideal Motion with Unsteady Aerodynamics

Steady aerodynamics require the motion of the airfoil up, down or rotation, to be much slower than the time it takes for the air to travel from the leading edge to the trailing edge. Unsteady aerodynamics accounts for this up and down motion or rotation. Because the motion of the blades are still considered to be the ideal inverse sine curve,

the angular rotation, and angular acceleration of the blades can be determined by differentiating the equation for the angular position. This is done as follows:

$$\begin{aligned}
 \alpha &= -\alpha_{Max} * \sin(\theta - \phi) \\
 \omega &= -\alpha_{Max} * \cos(\theta - \phi) * \frac{\partial \theta}{\partial t} = -\alpha_{Max} * \Omega * \cos(\theta - \phi) \\
 acc &= \alpha_{Max} * \Omega * \sin(\theta - \phi) * \frac{\partial \theta}{\partial t} = \alpha_{Max} * \Omega^2 * \sin(\theta - \phi)
 \end{aligned}
 \tag{Equation 12}$$

where  $\Omega$  is the rotational speed of the propeller. The 2-D unsteady lift and moment equations were taken from I. E. Garrick<sup>(5)</sup> for an airfoil with a flap or aileron, with the airfoil moving in a sinusoidal motion both vertically and rotationally. After the terms for the flap or aileron are removed, the equation becomes the following:

$$\begin{aligned}
 \frac{Lift}{Span} &= \rho * b^2 * \left[ \begin{array}{l} V_t * \pi * \alpha_0 * p * \cos(p * t + \phi_0) \\ - \pi * h_0 * p^2 * \sin(p * t + \phi_2) \\ + \pi * b * a * \alpha_0 * p^2 * \sin(p * t + \phi_0) \end{array} \right] \\
 + 2 * \pi * \rho * V_t * b * F &* \left[ \begin{array}{l} V_t * \alpha_0 * \sin(p * t + \phi_0) + h_0 * p * \cos(p * t + \phi_2) \\ + b * \left(\frac{1}{2} - a\right) * \alpha_0 * p * \cos(p * t + \phi_0) \end{array} \right] \\
 + 2 * \pi * \rho * V_t * b * G &* \left[ \begin{array}{l} V_t * \alpha_0 * \cos(p * t + \phi_0) - h_0 * p * \sin(p * t + \phi_2) \\ - b * \left(\frac{1}{2} - a\right) * \alpha_0 * p * \sin(p * t + \phi_0) \end{array} \right]
 \end{aligned}
 \tag{Equation 13}$$

where  $b$  is the semi chord (chord/2), 'a' is the pivot point for the blade (in this case it was set as the quarter chord) measured from the mid chord aft positive,  $p$  is the rotational speed of the propeller defined before as  $\Omega$ , and  $F$  and  $G$  are functions to reduce and phase shift the lift and moments.  $\alpha_0$ , and  $h_0$  are the magnitude of the assumed sinusoidal rotation motion and up and down motion, and  $\phi_0$  and  $\phi_2$  are the phase shifts of the corresponding sinusoidal motions of  $\alpha$  and  $h$ . Figure 6 shows these variables and there definitions. The variables  $F$  and  $G$  in equation 13 are the lift and moment attention and

phase shifts. To determine F and G, it is necessary to determine ‘k’, the reduced frequency of the oscillation. The following is the equation for k.

$$\kappa = \frac{\omega_{blade} * b}{Vel} = \frac{(650 RPM) * \left(\frac{1 ft}{2}\right)}{(2 ft) * (650 RPM)} = 0.25 \quad \text{Equation 14}$$

using the graph in figure 7, F was determined to be 0.7, and G was –0.19. Equation 13 was derived for a 2-D airfoil. Assuming that the only 3-D affect is in the lift curve slope, ‘ $2*\pi$ ’ can be replaced with the 3-D lift curve slope determined in equation 3. Since p is the rotational speed of the propeller,  $\Omega$ , and ‘t’ is time, ‘p\*t’ can be replaced with  $\theta$ , the position of the blade.  $\phi_0$  and  $\phi_2$  are both equal to the negative of the  $\phi$  defined in equation 1 and equation 12. Thus the equation reduce to the following:

$$\begin{aligned} \frac{Lift}{Span} = & \rho * b^2 * \left[ \begin{array}{l} -V_t * \pi * \alpha_{Max} * \Omega * \cos(\theta - \phi) \\ -\pi * h_{Max} * \Omega^2 * \sin(\theta - \phi) \\ -\pi * b * a * \alpha_{Max} * \Omega^2 * \sin(\theta - \phi) \end{array} \right] \\ + C_{L\alpha 3-D} * \rho * V_t * b * F * & \left[ \begin{array}{l} -V_t * \alpha_{Max} * \sin(\theta - \phi) + h_{Max} * \Omega * \cos(\theta - \phi) \\ -b * \left(\frac{1}{2} - a\right) * \alpha_{Max} * \Omega * \cos(\theta - \phi) \end{array} \right] \\ + C_{L\alpha 3-D} * \rho * V_t * b * G * & \left[ \begin{array}{l} -V_t * \alpha_{Max} * \cos(\theta - \phi) - h_{Max} * \Omega * \sin(\theta - \phi) \\ + b * \left(\frac{1}{2} - a\right) * \alpha_{Max} * \Omega * \sin(\theta - \phi) \end{array} \right] \end{aligned} \quad \text{Equation 15}$$

Once the lift is known, an educated guess on the drag of the blade can be made, if the lift coefficient is known. The lift coefficient is determined from the following equation.

$$C_l = \frac{Lift}{\frac{1}{2} * \rho * Vel^2 * S} \quad \text{Equation 16}$$

The induced drag coefficient can be determined using the standard equation for the drag polar, previously given as equation 6. Since equation 6 was also a ‘paper model’ of the cycloidal propeller, only the induced drag was used to model the blade drag. The drag is

determined using the definition of the drag previously given equation 7. The equation for the pitching moment required to rotate the blade due to the aerodynamic forces at a constant  $\Omega$ , is seen below:

$$\begin{aligned} \frac{M}{Span} = & -\rho * b^2 * \left[ \begin{array}{l} \pi * \left(\frac{1}{2} - a\right) * V_t * b * \alpha_0 * p * \cos(p * t + \phi_0) \\ -\pi * b^2 * \left(\frac{1}{8} + a^2\right) * \alpha_0 * p^2 * \sin(p * t + \phi_0) \\ + a * \pi * b * h_0 * p^2 * \sin(p * t + \phi_2) \end{array} \right] \\ & + 2 * \rho * V_t * b^2 * \pi * \left(\frac{1}{2} + a\right) * F * \left[ \begin{array}{l} V_t * \alpha_0 * \sin(p * t + \phi_0) + h_0 * p * \cos(p * t + \phi_2) \\ + b * \left(\frac{1}{2} - a\right) * \alpha_0 * p * \cos(p * t + \phi_0) \end{array} \right] \\ & + 2 * \rho * V_t * b^2 * \pi * \left(\frac{1}{2} + a\right) * G * \left[ \begin{array}{l} V_t * \alpha_0 * \cos(p * t + \phi_0) - h_0 * p * \sin(p * t + \phi_2) \\ - b * \left(\frac{1}{2} - a\right) * \alpha_0 * p * \sin(p * t + \phi_0) \end{array} \right] \end{aligned} \quad \text{Equation 17}$$

Again, the assumption that the only 3-D affect is in the lift curve slope will be used. The term ‘p\*t’ can be replaced with  $\theta$ , and ‘p’ can be replaced with  $\Omega$ .

$$\begin{aligned} \frac{M}{Span} = & -\rho * b^2 * \left[ \begin{array}{l} -\pi * \left(\frac{1}{2} - a\right) * V_t * b * \alpha_{Max} * \Omega * \cos(\theta - \phi) \\ + \pi * b^2 * \left(\frac{1}{8} + a^2\right) * \alpha_{Max} * \Omega^2 * \sin(\theta - \phi) \\ + a * \pi * b * h_{Max} * \Omega^2 * \sin(\theta - \phi) \end{array} \right] \\ & + C_{L\alpha 3-D} * \rho * V_t * b^2 * \left(\frac{1}{2} + a\right) * F * \left[ \begin{array}{l} -V_t * \alpha_{Max} * \sin(\theta - \phi) + h_{Max} * \Omega * \cos(\theta - \phi) \\ -b * \left(\frac{1}{2} - a\right) * \alpha_{Max} * \Omega * \cos(\theta - \phi) \end{array} \right] \\ & + C_{L\alpha 3-D} * \rho * V_t * b^2 * \left(\frac{1}{2} + a\right) * G * \left[ \begin{array}{l} -V_t * \alpha_{Max} * \cos(\theta - \phi) - h_{Max} * \Omega * \sin(\theta - \phi) \\ + b * \left(\frac{1}{2} - a\right) * \alpha_{Max} * \Omega * \sin(\theta - \phi) \end{array} \right] \end{aligned} \quad \text{Equation 18}$$

The pitching moment, along with moment due to inertia, can be used to compute the push-pull rod force. First, the normal acceleration of the blades due to centrifugal force must be known. The normal acceleration on the blades can then be found from the following kinematics equation.

$$a_n = \frac{V_t^2}{Radius} \quad \text{Equation 19}$$

Using Newton's second law, the resultant force can be found. Knowing the distance from the pivot point to the CG of the blade gives the resultant pitching moment due only to the normal acceleration. The rod force can then be determined using the following equation.

$$\text{Rod Force} = \frac{\text{Moment}_{\text{Aerodynamics}} + \text{Moment}_{\text{Centrifugal}} + \text{Moment}_{\text{AngularAcc}}}{P_d} \quad \text{Equation 20}$$

where  $P_d$  is the distance from the pivot point to the push-pull rod.

Since the lift, drag and pitching moment of each blade are known each blade's contribution to the propellers total lift and thrust can be calculated from equations 9 and 10. These can be summed for all blades at each theta using equation 11 to obtain the total lift and drag of the propeller.

There is an addition drag loss associated with the cycloidal propeller, associated with the blades producing an unsteady wake. An equation derived by I. E. Garrick<sup>(5)</sup> gives the power used in producing the wake and in maintaining the oscillation, and is given below as equation 21.

$$\dot{W} = \text{Lift} * \dot{h} + \text{Moment} * \dot{\alpha} \quad \text{Equation 21}$$

After equation 21 is added to equation 11, the torque and power become the following:

$$\begin{aligned} \text{Torque} &= \sum_{\text{Theta}=0}^{360} \sum_{\text{Number of blades}} \text{Drag} * \text{Radius} + \frac{\text{Lift} * \dot{h} + \text{Moment} * \dot{\alpha}}{\Omega} \\ \text{Power} &= \sum_{\text{Theta}=0}^{360} \sum_{\text{Number of blades}} \frac{\text{Drag} * V_t}{550} + \text{Lift} * \dot{h} + \text{Moment} * \dot{\alpha} \end{aligned} \quad \text{Equation 22}$$

## Real Motion with Unsteady Aerodynamics

The real motion of the blades is based on a collection of four bar linkages controlling the individual blades commanded blade angle. By offsetting one point common to all of the blades, the maximum AoA as well as the direction of Lift/Thrust can be determined. Figure 8 shows the four bar linkage system. This linkage system was chosen because it is a good match for the ideal sine motion, however, it does diverge from the ideal motion at large AoA.

Figure 9 shows the AoA for both the ideal motion and the four bar linkage motion. If the AoA's for the real motion and the ideal motion are matched at theta equals  $270^\circ$ , the angle at theta equals  $90^\circ$  is greater for the real motion than it is for the ideal motion. There is also a phase lag in the curve of about  $8^\circ$ . There is one advantage to the four bar linkage producing a larger AoA at  $90^\circ$ . When the cycloidal propeller is producing lift, the blade at  $90^\circ$  needs to be at a larger AoA because of down wash. The phase shift will be discussed later in the next section.

The next step is to observe the mechanics of the four bar linkage system. For simplicity, only one four bar linkage will be examined. Figure 10 shows a four bar linkage with the lengths, and angles that will be discussed later. Using the following equations from the text book "Design of Machinery"<sup>(6)</sup>, the angles, angular velocities, and angular accelerations can be determined for each of the links of the four bar linkage:

$$A = \cos(\theta_2) - \frac{L_1}{L_2} - \frac{L_1}{L_4} * \cos(\theta_2) + \frac{L_2^2 - L_3^2 + L_4^2 + L_1^2}{2 * L_2 * L_4}$$

$$B = -2 * \sin(\theta_2)$$

$$C = \frac{L_1}{L_2} - \left( \frac{L_1}{L_4} + 1 \right) * \cos(\theta_2) + \frac{L_2^2 - L_3^2 + L_4^2 + L_1^2}{2 * L_2 * L_4}$$

$$D = \cos(\theta_2) - \frac{L_1}{L_2} - \frac{L_1}{L_3} * \cos(\theta_2) + \frac{L_4^2 - L_1^2 - L_2^2 + L_3^2}{2 * L_2 * L_3}$$

$$F = \frac{L_1}{L_2} + \left( \frac{L_1}{L_3} - 1 \right) * \cos(\theta_2) + \frac{L_4^2 - L_1^2 - L_2^2 + L_3^2}{2 * L_2 * L_3}$$

$$\theta_4 = 2 * a \tan \left( \frac{-B - \sqrt{B^2 - 4 * A * C}}{2 * A} \right)$$

$$\theta_3 = 2 * a \tan \left( \frac{-B - \sqrt{B^2 - 4 * D * F}}{2 * D} \right)$$

$$\omega_4 = \frac{L_2 * \omega_2 * \sin(\theta_4 - \theta_2)}{L_3 * \sin(\theta_3 - \theta_4)}$$

$$\omega_3 = \frac{L_2 * \omega_2 * \sin(\theta_2 - \theta_3)}{L_4 * \sin(\theta_4 - \theta_3)}$$

$$AA = L_4 * \sin(\theta_4)$$

$$BB = L_3 * \sin(\theta_3)$$

$$CC = L_2 * \alpha_2 * \sin(\theta_2) + L_2 * \omega_2^2 * \cos(\theta_2) + L_3 * \omega_3^2 * \cos(\theta_3) - L_4 * \omega_4^2 * \cos(\theta_4)$$

$$DD = L_4 * \cos(\theta_4)$$

$$EE = L_3 * \cos(\theta_3)$$

$$FF = L_2 * \alpha_2 * \cos(\theta_2) - L_2 * \omega_2^2 * \sin(\theta_2) - L_3 * \omega_3^2 * \sin(\theta_3) + L_4 * \omega_4^2 * \cos(\theta_4)$$

$$\alpha_3 = \frac{CC * DD - AA * FF}{AA * EE - BB * DD}$$

$$\alpha_4 = \frac{CC * EE - BB * FF}{AA * EE - BB * DD}$$

**Equation 23**

These equations are found in most mechanism books and are considered standard equations for an open four-bar linkage. For this problem, there are several changes;  $\theta_2$  is the driving angle and is measured from the vertical, counter clockwise to link 2, the  $\theta$  defined before is measured from the X-axis, counter clockwise, and the difference between  $\theta$  and  $\theta_2$  is  $90^\circ$ . From figure 8, the offset is a negative number. All of the

aerodynamics assumes the oscillation is quasi-steady and neither speeding up nor slowing down, which means that  $\alpha_2$  must equal zero.

The angle needed from this calculation is the commanded blade angle,  $\beta$ .  $\theta_3$  is the angle measured from the vertical to the link 3.  $\beta$  can then be defined as the angle from link 2 to link 3 minus  $90^\circ$ , and  $\beta$  was determined to be equal to  $\theta - \theta_3$ . For the same reason, the angular velocity as measured relative to link 2 is  $\Omega - \omega_3$ .

Since the AoA, angular velocity, and angular accelerations are known, the aerodynamic forces can be found. The only major difference resides in the unsteady lift and moment equations. If this computer modeling was to be done strictly ‘by the book’ a Fourier fit would be done using the real motion, and the motion would be modeled as a series of sinusoids. As a first order approximation, the calculated AoA, angular velocity, and angular acceleration were placed into equations 15 and 18. Equation 15 then reduced to the following equation:

$$\begin{aligned} \frac{Lift}{Span} = & Lift_{Apparent\ Mass} + Lift_{Circulatory\ Real} + Lift_{Circulatory\ Imaginary} = \\ & \rho * b^2 * \left[ V_t * \pi * \dot{\alpha} + \pi * \ddot{h} - \pi * b * a * \ddot{\alpha} \right] \\ & + C_{L\alpha\ 3-D} * \rho * V_t * b * F * \left[ V_t * \alpha + \dot{h} + b * \left( \frac{1}{2} - a \right) * \dot{\alpha} \right] \\ & + \frac{C_{L\alpha\ 3-D} * \rho * V_t * b * G}{\Omega} * \left[ V_t * \dot{\alpha} + \ddot{h} + b * \left( \frac{1}{2} - a \right) * \ddot{\alpha} \right] \end{aligned} \quad \text{Equation 24}$$

Accordingly, equation 18 reduced to the following equation:

$$\begin{aligned}
\frac{M}{S_{pan}} &= \text{Moment}_{\text{Apparent Mass}} + \text{Moment}_{\text{Circulatory Real}} + \text{Moment}_{\text{Circulatory Imaginary}} = \\
&- \rho * b^2 * \left[ \pi * \left( \frac{1}{2} - a \right) * V_i * b * \dot{\alpha} - \pi * b^2 * \left( \frac{1}{8} + a^2 \right) * \ddot{\alpha} - a * \pi * b * \ddot{h} \right] \\
&+ C_{L\alpha 3-D} * \rho * V_i * b^2 * \left( \frac{1}{2} + a \right) * F * \left[ V_i * \alpha + \dot{h} + b * \left( \frac{1}{2} - a \right) * \dot{\alpha} \right] \\
&+ \frac{C_{L\alpha 3-D} * \rho * V_i * b^2 * \left( \frac{1}{2} + a \right) * G}{\Omega} * \left[ V_i * \dot{\alpha} + \ddot{h} + b * \left( \frac{1}{2} - a \right) * \ddot{\alpha} \right]
\end{aligned} \tag{Equation 25}$$

With these lift and moment equations, the calculation of the propellers total lift and thrust remain the same. Using equations 9 and 10, each blade's contribution to the propellers lift and thrust can be found. Using equation 22, the torque and power required by the propeller can be found.

The phase shift in the commanded blade is inherent in a four bar linkage system. The length of the push rods, L4 in figure 10, was set such that when the offset is zero, the commanded blade angle  $\beta$  is zero for all thetas. When the offset is moved up or down,  $\beta$  is no longer zero at theta equal to  $0^\circ$  or at  $180^\circ$  as seen in figure 9. The magnitude of this error was sufficiently small to continue using the four bar linkage system. There is an easy fix;  $\phi$  rotates the lift vector by rotating the point at where the  $\beta$  is zero. To remove the phase shift, simply rotate  $\phi$  slightly and the commanded blade angle can be reset to zero at theta equals zero.

## CHAPTER III

### DYNAMIC EFFECTS

#### Forward Motion

Forward speed on the propeller has only one effect; to change the individual blades AoA. To model this effect an equation was developed to calculate the induced angle of attack, AoAW. This equation is derived in this section, but first, in true helicopter fashion, the advance ratio is defined using the following equation.

$$k = \frac{\sqrt{(V_x)^2 + (V_z)^2}}{V_t} \quad \text{Equation 26}$$

Figure 11 shows the blade at several different points, with vectors denoting the tip velocity, the cycloidal propeller's velocity in the X direction, and the velocity in the Z direction. Vr is the resultant velocity on the blades, with AoA being the angle of attack induced by the forward motion. The following table was made from examining the tangential and normal velocity induced on the blades at different thetas. From the resultant velocity, Vr, and the AoA induced by the wind can be found. The derivation of the appropriate equation can be seen in table 1.

Table 1. Derivation of Induced AoA Equation

Theta	$V_{\text{tangent}}$	$V_{\text{normal}}$	$V_r$	AoA of wind
0°	$V_{\text{tip}} - V_z$	$V_x$	$\text{Sqrt}(V_{\text{tangent}}^2 + V_{\text{normal}}^2)$	$\text{atan}(V_{\text{normal}}/V_{\text{tangent}})$
90°	$V_{\text{tip}} - V_x$	$-V_z$	$\text{Sqrt}(V_{\text{tangent}}^2 + V_{\text{normal}}^2)$	$\text{atan}(V_{\text{normal}}/V_{\text{tangent}})$
180°	$V_{\text{tip}} + V_z$	$-V_x$	$\text{Sqrt}(V_{\text{tangent}}^2 + V_{\text{normal}}^2)$	$\text{atan}(V_{\text{normal}}/V_{\text{tangent}})$
270°	$V_{\text{tip}} + V_x$	$V_z$	$\text{Sqrt}(V_{\text{tangent}}^2 + V_{\text{normal}}^2)$	$\text{atan}(V_{\text{normal}}/V_{\text{tangent}})$

Given that the motion is based on a sinusoidal variation from theta to theta an equation for  $V_{\text{tangent}}$  and  $V_{\text{normal}}$  is derived as follows:

$$\begin{aligned} V_{\text{Tangent}} &= V_{\text{Tip}} - V_z * \cos(\theta) - V_x * \sin(\theta) \\ V_{\text{Normal}} &= V_x * \cos(\theta) - V_z * \sin(\theta) \end{aligned} \quad \text{Equation 27}$$

Equation 27 can also be derived using the coordinate transformation from a rotating to a stationary coordinate system, previously listed as equation 8. After equation 8 is rearranged to transform a stationary to a rotating coordinate system, rotating about the Y-axis, following set of equations are appropriate:

$$\begin{aligned} i_{\text{Rotating}} &= i_{\text{Fixed}} \sin(\varphi) + j_{\text{Fixed}} \cos(\varphi) \\ j_{\text{Rotating}} &= j_{\text{Fixed}} \\ k_{\text{Rotating}} &= -i_{\text{Fixed}} * \cos(\varphi) + j_{\text{Fixed}} * \sin(\varphi) \end{aligned} \quad \text{Equation 28}$$

When the rotating velocity  $V_{\text{tip}}$ , the negative of the forward motion velocity,  $V_x$  and  $V_z$ , are put into equation 28 equation 27 emerges. The resultant velocity can be calculated using the Pythagorean Theorem seen below as equation 29.

$$V_r = \sqrt{(V_{\text{Tangent}})^2 + (V_{\text{Normal}})^2} \quad \text{Equation 29}$$

The induced AoA caused by forward speed is given as equation 30.

$$AoAW = a \tan\left(\frac{V_{\text{Normal}}}{V_{\text{Tangent}}}\right) \quad \text{Equation 30}$$

For advance ratios greater than 1, care must be taken to insure that the AoA is placed in the correct quadrant. The total angle of attack that the blades are experiencing is the sum of the commanded blade angle and the induced angle.

$$\alpha = \beta_{Commanded} + AoAW \quad \text{Equation 31}$$

Once the total AoA of the blade is known, the lift, drag, pitching moment, resultant force in the X and Z directions can be determined.

### Downwash

Since there is now an equation that allows for air flowing towards the propeller, the uniform downwash velocity can now be computed. Because the induced wind velocity is directly related to the amount of lift that the propeller is generating, and the lift is directly related to the induced velocity of the air around the propeller, an iterative scheme must be employed to solve for the lift or thrust generated. Using helicopter momentum theory (actuator disk theory), the induced velocity of the air through the propeller is given by the following equation <sup>(7)</sup>.

$$\begin{aligned} V_{induced\_Z} &= \sqrt{\frac{Lift}{2 * \rho * Const * A}} = \sqrt{\frac{Lift}{2 * \rho * Const * (Span * Diamiter)}} \\ V_{induced\_X} &= \sqrt{\frac{Thrust}{2 * \rho * Const * A}} = \sqrt{\frac{Thrust}{2 * \rho * Const * (Span * Diamiter)}} \end{aligned} \quad \text{Equation 32}$$

where A is the projected area of the cycloidal propeller. The constant multiplier of the area occurs because the cycloidal propeller has blades at the top and bottom and acts like a uniaxial counter rotating tandem rotor helicopter. However, the blades are not producing the same amount of lift at the edges of the projected area, so the constant

should be between 1.0 and 2.0. This constant will be adjusted to fit the test data. After matching the program output to the experimental data, the constant was found to equal 1.7.

### Wind Gusts

It was determined that when the cycloidal propeller is trimmed for hover, the propeller is very susceptible to gusts. This is shown in figure 11; if  $V_z$  is zero and  $V_x$  is any positive number, then there is an induced AoA on the blades at theta equal to  $0^\circ$  and  $180^\circ$ . This induced AoA produces a force in the same direction as a wing gust. This retarding force which is drag, is plotted as a function of the velocity of the wind gust in figure 12.

This wind gust also decreases the lift of the propeller. This is because of the induced AoA at theta equals to  $0^\circ$  and  $180^\circ$  at the same time that there is an induced AoA at theta equals to  $90^\circ$  and  $270^\circ$  because of the downwash. The decrease in lift is plotted in figure 13.

Because the propeller is producing less lift, it should require less power than it did in the trim position. Figure 14 shows that decrease in power.

### Forward Motion by Rotating Phi

An effort was made to determine the amount of  $\phi$  and increase or decrease in the offset required to trim the propeller for a given forward flight speed, assuming the only

source of drag is the propeller. Figure 15 shows the commanded  $\phi$  required to null the drag produced by the gust.

With the total lift force produced by the propeller rotated into the wind, the offset must also be increased to make enough lift to keep the propeller in the air. The figure 16 shows the offset needed as a function of the forward speed. For hovering, the maximum commanded blade angle is  $45.1^\circ$  and the maximum AoA of the blades is  $25.5^\circ$ . For a forward velocity of 50 MPH, the maximum commanded blade angle is  $47.3^\circ$ , and the maximum AoA of the blade is  $24.5^\circ$ . The offset has to be increased to this degree because the propeller has to take bigger and bigger bites to keep the same total AoA profile. Figure 17 shows the HP required to hold the propeller stationary against the wind.

### Cam Shapes Required for Forward Motion

As an “exercise for the student,” the writer was asked to determine the cam shape needed to neutralize the induced AoA caused by different velocities in the X direction. Figure 18 shows the different cam shapes needed for an advance ratio of 0.5 and 1.5.

For advance ratios less than 0.5, the cam shape is reasonable and easy for a cam follower to follow. For advance ratios, greater than 1.5, the cam shape is also reasonable, but requires some help in the form of a clicker or stop to make the blade swap from a cam follower to a cam leader and back to a cam follower. The problem comes at advance ratios between 0.5 and 1.5. Figure 19 shows the cam shape for several advance ratios from zero to two.

There is a 'no-mans-land' at theta equal to  $90^\circ$ , due to retreating blade stall. As  $k$ , the advance ratio, approaches 1, the airspeed over the blade is approaching zero, and the blade does not know which direction to point. At  $k$  equals 1, the AoA induced by the wind is undefined. It still may be possible to have two cams, one to roughly neutralize the induced AoA at  $k$ 's less than 0.5, and another cam that roughly neutralizes the induced AoA at  $k$ 's greater than 1.5. In this case the propeller may simply power through the retreating blade stall, switch gears, and proceed to higher advance ratios. This may be investigated further at a later date, but currently, more concerns exist with hover and slow speed flight. The system that has been developed can easily go to advance ratios approaching 0.5, which appears to be sufficient given the scope of this work.

## CHAPTER IV

### COMPARISON OF COMPUTER MODEL WITH WHEATLEY WIND TUNNEL DATA

In the 1930's a leader in the field of cycloidal propulsion was John B. Wheatley. In one of his papers<sup>(2)</sup> he performed extensive wind tunnel tests of a propeller he developed. This cycloidal propeller was placed in the 20-foot wind tunnel at the now NASA Langley. In this paper<sup>(2)</sup> Wheatley does extensive static wind tunnel testing of the cycloidal propeller for the forces in the Z and X direction as well as the power required by the propeller, as a function of the maximum AoA, and the propellers rotation speed. In this thesis, Wheatley's cycloidal propeller was modeled using the "Real Motion Unsteady Aerodynamics" computer program. The results are compared to Wheatley's data in figures 20-22.

Figures 20 and 21 show the force in the Z and X direction produced by the propeller as a function of the maximum AoA for three different rotational speeds. The lines with circles show the Wheatley's experimental data, and the lines with no circles are the calculated results from the cycloidal propeller program. Since the lift of a blade is directly proportional to the AoA of the blade as shown by equations 4 and 5, it follows that the forces in the Z and X direction are linear with the maximum AoA. The lift is proportional to the square of the local velocity, and the velocity is directly proportional to

the rotational speed, so forces in the X and Z direction are proportional to the square of the rotational speed. The influence of both the AoA and rotation speed can be seen in the figure 20 and 21.

Figure 22 shows the power required by the propeller as a function of the maximum AoA, for three different rotational speeds. The lines with circles show the Wheatley's experimental data, and the lines with no circles are the calculated results from the cycloidal propeller program. The drag of the blade is related to the square of the AoA, and since the drag of the blades is the dominant factor in the power required by the propeller, it follows that the power should be proportional to the square of the maximum AoA. The drag of the blade is proportional to the square of the local velocity, and the velocity is directly proportional to the rotational speed. The power required by the propeller is proportional to the local velocity and the drag of the blade; thus the power required by the propeller is proportional to the cube of the rotational speed. The influence of both the AoA and the rotational speed can be seen in figure 22.

Wheatley also tested the cycloidal propeller at different forward speeds and developed a curve for the horsepower to lift ratio as a function of the forward speed. To verify the computer model that was developed Wheatly's wind tunnel data was reproduced. Figure 23 shows the experimental data from Wheatley's cycloidal propeller and Wheatley's calculated results as well as the results from the cycloidal propeller program. The data matches reasonably well; the computed HP/Lift ratio is slightly high at about 50 mph of forward speeds, compared to Wheatley's data, indicating the computer program is either over estimating the power required, or under estimating the lift.

## CHAPTER V

### COMPARISON OF MODEL WITH EXPERIMENT

#### Cycloidal Propeller designed for Bosch Aerospace

The cycloidal propeller designed by Bosch Aerospace and Raspet Flight Research

Laboratory had the following design variables,

Airfoil section – NACA 0012

Diameter – 4 ft

Span of the blades – 4 ft

Number of Blades – 6

Chord of the blades – 1 ft

Rotational Speed – 650 RPM

#### **Airfoil**

The NACA 0012 appears to be a very good airfoil for this application. It has a good lift curve slope and good stall characteristics. The airfoil may be changed at a later date to the NACA 0015, to allow a larger spar to be placed in the blade.

#### **Diameter**

Since larger is better, a diameter of four feet was chosen since this was the maximum diameter that could fit on the proposed VTOL UAV.

**Span**

Kerstin's <sup>(1)</sup> suggestion of making the span equal to the diameter was taken and the span was set as four feet.

**Number of Blades**

A six-bladed propeller was chosen because it gave the vibration frequency of six times the rotational speed, and it allows more than one blade to produce the required instantaneous lift. This smoothed out the cycloidal propeller considerably.

**Chord**

Choosing a chord of one foot gave roughly one chord length between each blade. This made the circumference half blade, and half free air.

**Speed of Rotation**

Given that all of the previous variables were set by other constraints or by logical choices,  $\Omega$  was the only variable left to choose. For this case, it was determined that the required lift of 350 lb required the propeller to turn at 650 RPM, with a tip speed at about 140 ft/s.

### Comparison of Different Computer Models

For comparison, the variables listed above were used and the maximum commanded blade angle at  $270^\circ$  were set at  $25^\circ$  for all three cases. This means the angle of attack is roughly the same for both cases. The mechanical phase shift associated with the four bar linkage system was not taken out by rotating  $\phi$ .

Figure 9 shows the angle of attack of the ideal motion and the real motion. The AoA of both the ideal motion and the four bar linkage motion match reasonably well. If the AoA's at theta equal to  $270^\circ$  are matched for all three cases, then the four bar linkage system produces a larger AoA at  $90^\circ$ . This is actually a good thing because it will help with down wash. There is also a phase lag of about  $8^\circ$ , inherent in the four bar linkage system.

Figure 24 shows the angular velocities for both the ideal motion and the real motion. The angular velocities were calculated using equation 12 for the ideal motion and equation 23 for the four-bar linkage motion. The velocities are quite large.

Figure 25 shows the angular acceleration of the blade. The angular velocities were calculated using equation 12 for the ideal motion and equation 23 for the four-bar linkage motion. The acceleration of the blade is quite high. Not only does the blade have to resist a 300g bending moment, but it also has to resist a 25g torsional moment. These blades will have to be very stiff and strong, and there may also be some aerodynamic/inertial elastic effects that require attention.

Figure 26 shows the induced AoA caused by the downwash. There is no downwash in the Ideal Motion Steady Aerodynamics, and in the Real Motion with no downwash cases. This induced AoA tends to washout the commanded blade angle. This can be seen in figure 27.

Figure 27, shows the total AoA of the blade. The total AoA is the commanded blade angle plus the induced AoA. The downwash reduced the AoA from  $\pm 25^\circ$  to approximately  $\pm 10^\circ$ .

Figure 28 shows the lift of a blade modeled with steady and unsteady aerodynamics. If approached correctly, unsteady aerodynamics can produce a substantial increase in performance. If the conditions are not optimum, unsteady aerodynamics can also hurt the performance. There is approximately a 100% gain in lift due to unsteady aerodynamics with no downwash. When the downwash is included the lift drops back down to approximately the same as the Ideal Motion Steady Aerodynamics case. There is also a substantial phase shift associated with the real motion with no downwash. The AoA has a lagging phase shift of about  $8^\circ$ , and the lift has a leading phase shift of  $1^\circ$ . This means unsteady aerodynamics alone has a phase shift of  $9^\circ$ . In this plot, the influence of the larger AoA at  $90^\circ$  is apparent. The real motion with down wash has another phase shift. At  $90^\circ$  there is a phase lag of  $28^\circ$  and at  $270^\circ$  there is a phase lead of  $28^\circ$ . This is caused by the induced AoA and can be seen in figure 26.

Figure 29 shows the drag of the blade modeled with Ideal Motion Steady Aerodynamics and Real Motion Unsteady Aerodynamics with and without downwash. This drag is only the induced drag produced by the blade; thus it should have the same characteristics as the lift curve. In this plot, the phase shift and the influence of the larger bite at  $90^\circ$  is apparent.

Figure 30 shows the force in the Z direction produced by the blade, modeled by both steady and unsteady aerodynamics, both with and without downwash. The force in the Z direction is the propellers lift. It is roughly the absolute value of the lift of the blade. As such, the same characteristics in this plot are observed in the rest of the plots. There is a phase shift caused by unsteady aerodynamics, and a larger peak at  $90^\circ$  than at

270°. It is noted that the force in the Z direction is not zero at theta equal to 0°, or 180°. This result is because the equation for the force in the Z direction, equation 10, takes into account the drag as well as the lift. At theta equals 0°, the drag is producing a force in the positive Z direction, at 180°, and the drag is producing a force in the negative Z direction. This can be seen in figure 30.

Figure 31 shows the force in the X direction for both the steady and unsteady aerodynamic models with and without downwash. This plot requires more explanation; the reason the peaks of the curve occur at or around intervals of 45° is because the equation for the force in the X direction, equation 9, takes into account the lift and the drag. At intervals of 45°, the lift and drag either add together or take away from each other. Figure 5 shows the blades at intervals of 45°, the following table was made from that drawing:

Table 2. Magnitude of Blade force in X Direction

Theta	$F_x$	$F_x$ with lift larger than drag
45°	Drag-Lift	Small (-)
135°	Lift+Drag	Large (+)
225°	-Lift-Drag	Large (-)
315°	Lift-Drag	Small (+)

This corresponds with figure 31. The peaks and valleys do not occur exactly at intervals of 45° because the interaction of the lift and the drag are both changing as a

function of theta. The following table shows the other variables calculated by the computer model:

Table 3. Program output that is not a Function of Theta

Variable	Ideal Motion Steady Aerodynamics	Real Motion Unsteady Aerodynamics With No Downwash	Real Motion Unsteady Aerodynamics With Downwash
Average Lift (in Z direction)	296.25 lbs	554.7 lbs	170.53 lbs
Average Thrust (in X direction)	0 lbs	50.99 lbs	0.22lbs
Average Torque	370 ft-lbs	711.8 ft-lbs	317.57 ft-lbs
Average Power	45.78 HP	90.47 HP	41.9
Total Force	296.25 lbs	557.04 lbs	170.53 lbs

The computer model with ideal motion produces a symmetric curve for the force in the X direction. This explains why when the forces in the X direction are summed, the average is zero. The computer model does not produce a symmetric curve for the force in the X direction, partly because of the mechanical motion and partly because of unsteady aerodynamic effects. The result is a net force in the X direction. This force can easily be controlled by adjusting  $\phi$ , until the force is zero.

## Testing History

### **Test Rig**

To validate the computer model made at Raspet Flight Research Laboratory, Bosch Aerospace constructed a cycloidal propeller test rig. This test rig is capable of

measuring the lift, RPM, and torque needed by a cycloidal propeller. A sketch of the rig is given in figure 32. The relevant data at this time is the torque and power required to generate lift. To collect the data, there were three load cells mounted on the test rig. Two on the end of the outriggers and one mounted on the engine cradle. By summing the two load cells mounted at the end of the outrigger, the lift can be measured. The test rig was designed so that the engine was slung under the propeller. Figure 33 shows a sketch of the rig and the under slung engine.

With the engine able to swing, the torque required to turn the propeller also rotates the engine swing. With a load cell mounted a known distance below the propeller drive shaft, the torque absorbed by the propeller and drive train can be measured. As a check of the torque measured using the under-slung engine and its load cell, the torque was also measured by looking at the difference in the loads measured by load cells mounted at the end of the outrigger. With the exception of a few anomalous points, the data between the two match very well.

### **Blades**

The first-generation blades for the cycloidal propeller were made of aluminum, and were rib and skin construction. The skin was tack welded onto the ribs, and there was a half-span spar made of 4130 stainless steel. This spar ran from the half span mark on one side to the half span mark on the other side to carry the bending moment of the blades. There was a problem associated with this system; because the blades had a gap between the two sides, the blades essentially have an aspect ratio of only a half span. The blades weighted approximately three lbs each, or six lbs per pair. This set of blades proved to be inadequate for the g loading environment to which they were exposed.

When running the propeller, the blades would bow and produce several degrees of dihedral. Tack welding the skins to the ribs also proved to be inadequate; during one test the top skin of one blade actually peeled off the ribbed substructure. There were also several weld breaks on other blades.

Because of these problems, it was decided that a second-generation blade set was needed. These blades were constructed of foam core, carbon woven skins, and were one piece (full span). It was thought that this would alleviate the bending problem and give a full span aspect ratio, but it introduced several other problems. In order to connect the blade to the existing propeller, two large holes had to be cut in the blade, one for mounting at the  $\frac{1}{4}$  chord for a pivot point, and one to mount the push-pull rod. A 4130 stainless steel tube was used to carry the shear from the blade to the propeller arm. This carry through member slid inside the blade, through the propeller arm, and into the other side of the blade.

Because of the two holes cut in the blade for mounting, the blade was also structurally weaker. Two failures were associated with this. One was a catastrophic failure in which the blade broke into two pieces at the shear web where the mounting hole was cut. Each side of the blade then slid off the carry through member. The other failure involved the bottom skin of the blade breaking in tension at high RPM.

Because of this, it was decided to make a third-generation blade set. These will be full length blades, but the pivot point will be moved from the  $\frac{1}{4}$  chord, to the CG of the airfoil, and the pivot point will be moved down, and out of the blades, so that the blade can have a full length carbon spar. These blades will be constructed in the future.

### **Push-Pull Rods**

The pitching moment, along with moment due to inertia, can be used to compute the push-pull rod force. Figure 34 shows the pivot point, the airfoils CG, and the location of the push-pull rod for the blades. These blades are turning at 650 RPM, which is equal to 68 r/s. The radius of the propeller is two feet; therefore the tip speed is 136ft/s. The normal acceleration on the blades can then be found from the kinematics equation listed as equation 19.

It was found that the normal acceleration on the blades when the propeller is spinning at 650 RPM is 9,266 ft/s<sup>2</sup>. This is equal to 288 g's! The second-generation blades that were constructed weighed eight lbs. This means that at operating RPM the blades must support 2,300lbs. With the pivot point not at the CG of the blade, the push-pull rod has to support roughly half of the 2,300 lbs. Taking the sum the moments about the pivot point, the push-pull rods have to support 900 lbs, in addition to the aerodynamic pitching moments produced by the blade. At operating RPM and AoA, the pitching moments produce about  $\pm 100$  lbs in the push-pull rods. The rods are now exposed to a cyclic load of 800 lbs to 1000 lbs. The frequency of the loading is one per rev, and it does not take long for fatigue to appear. A simple solution to the problem involves making the third-generation blades with the pivot point at the CG of the airfoil. This will remove the inertia loads from the push-pull rods.

### **Comparison of the Computer Model and Test Data**

Data was collected with the cycloidal propellers second-generation blades. Figure 35 shows the lift generated as a function of RPM for the computer predictions and the

measured lift from the propeller. The curve with the circles is the test data, and the circles are actual data points. The dashed line is the computer predictions using the Real Motion Unsteady Aerodynamics with Downwash. As seen in the figure, this data fits the measured data very well.

Figure 36 shows the power required by the propeller, as well as the computer predictions. There are two test data curves. The solid curve with the circles, shows the horsepower (HP), measured with the load cell on the swinging engine cradle, and the solid curve with the diamonds is the HP measured with the differential lift method. There is good agreement between the two measurements of power, with the exception of a few stray points. The dashed curve in figure 36 is the computer prediction. After comparing the Wheatley data to the computer program and examining the Bosch cycloidal propeller, it was found that the  $C_{D0}$  of the propeller was much higher than originally assumed. To match the power data shown in figure 36, the  $C_{D0}$  of the blades was adjusted, to 0.07. This is not unreasonable, the arms of the propeller are essentially flat plates that are 2” wide and extend from a radius of 0.5 foot to 2 feet. When this drag alone is summed and lumped to the blades, the  $C_{D0}$  is equal to 0.042. When the interference drag, and the natural  $C_{D0}$  of the blade is added, the total  $C_{D0}$  would approach the value of 0.07.

## CHAPTER VI

### CONCLUSIONS

The purpose of his project was to create a computer model of a cycloidal propeller, and then compare the predictions with the actual performance of a cycloidal propeller. To do this, three computer programs were created. One used an ideal sine motion of the blades, with steady aerodynamics. The next program kept the ideal motion and used unsteady aerodynamics developed by I. E. Garrick. The final program used the real motion of the cycloidal propeller combined with unsteady aerodynamics both with and without downwash.

The real motion with unsteady aerodynamics with downwash was then compared to test data taken from a cycloidal propeller constructed by Bosch Aerospace. The computer predictions agree well with measured lift and HP.

In the process of testing the first and second-generation blades on the cycloidal propeller, much was learned about the fatigue nature of the cycloidal propeller. Testing of the first-generation blades on the cycloidal propeller showed that stiff blades were needed to avoid excessive dihedral produced by centrifugal loads. It was also learned that tack welded aluminum does not have the fatigue resistance needed to survive in this loading environment.

The second-generation blades were made of carbon fiber and were quite a bit stiffer than the first-generation blades. However, to mount the blades to the existing

cycloidal propeller, two large holes had to be cut in the center of the blade. This proved to fatally weaken at least one blade and caused the failure of another in different test runs.

A third-generation blade is in the design phase and will incorporate all the lessons learned in the previous blade sets. The biggest change will be to move the pivot point closer to the CG of the airfoil in order to unload the push-pull rods. The other major design change will be to move the pivot point outside of the blade to allow the blade to have a full-length spar. Other small changes are also being considered.

It may have noticed that the commanded blade angles are quite large for a cycloidal propeller; this is because the downwash through the propeller tends to washout the AoA of the blade. During tuft testing of the cycloidal propeller, the stall commanded blade angle was determined to be approximately  $32^\circ$  at 500 RPM. Further work on stall commanded blade angle as a function of RPM is planned.

The comparison of the computer model to the Wheatley data showed the forces to be with 10% and the power to be with 15%. Comparison with the Bosch Aerospace test data showed the forces to be within 5% for the lift and power.

## BIBLIOGRAPHY

- (1) Kirsten, Fredric, Cycloidal Propulsion Applied to Aircraft Transaction of the American Society of Mechanical Engineers, AER-50-12, pp. 25-48.
- (2) Wheatley, John B. and Windler, Ray, Wind Tunnel Tests of a Cyclogiro Rotor, NACA Technical Note 528, pp. 1-29
- (3) Abbot and Von Doenhoff , Theory of wing sections, Dover Publications 1959
- (4) Etkin and Reid, Dynamics of Flight, John Wiley & sons, 1996
- (5) I. E. Garrick, Propulsion of a flapping and Oscillating Airfoil, NACA Report No. 567, pp. 419-427
- (6) Norton, Robert L., Design of Machinery, Magraw-Hill, New York, New York.
- (7) Prouty, W. Raymond, Helicopter Performance, Stability, and Control, Krieger Publishing company, Malabar, FL, 1995

## APPENDIX A

### FIGURES

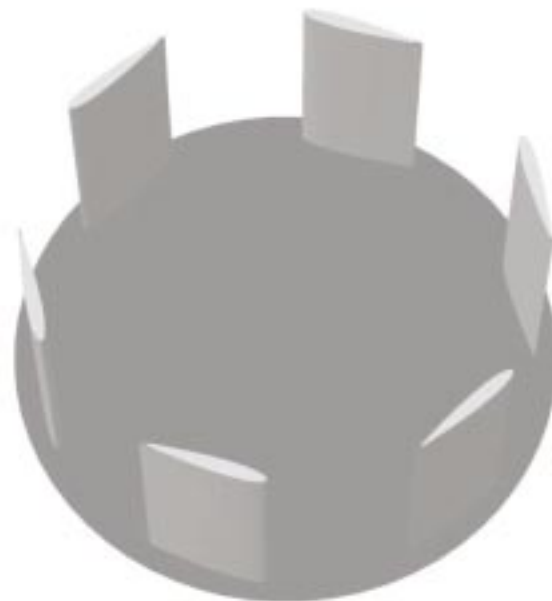


**Figure 1. Cantilevered Cycloidal Propeller**

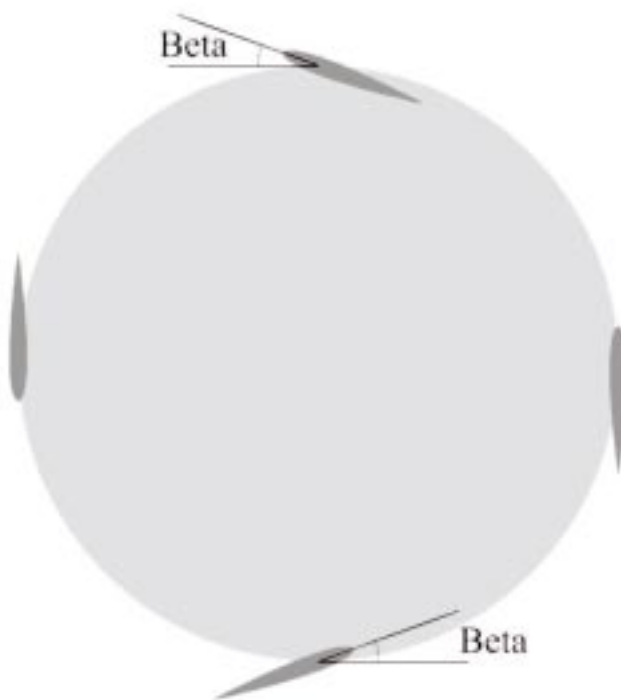


**Figure 2. Commanded Blade Angle**

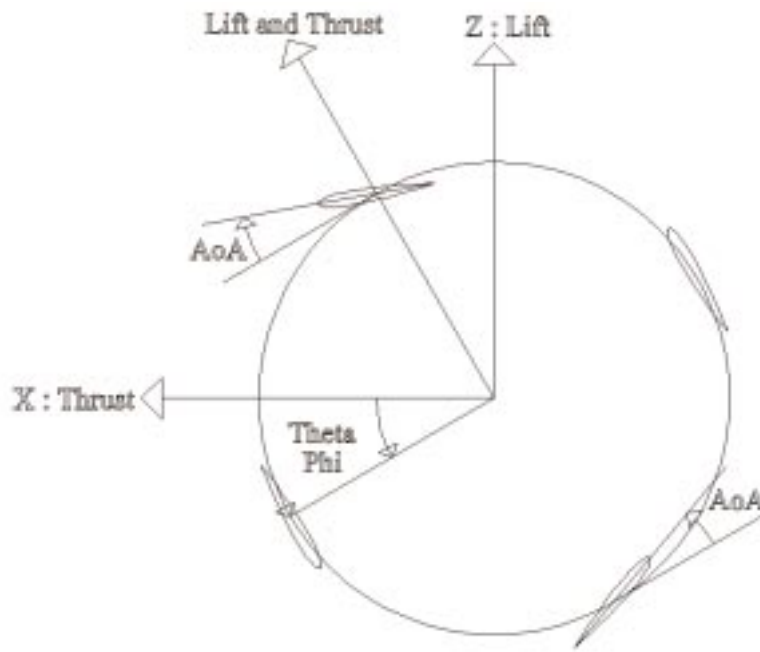


**Figure 3. Coordinate System**

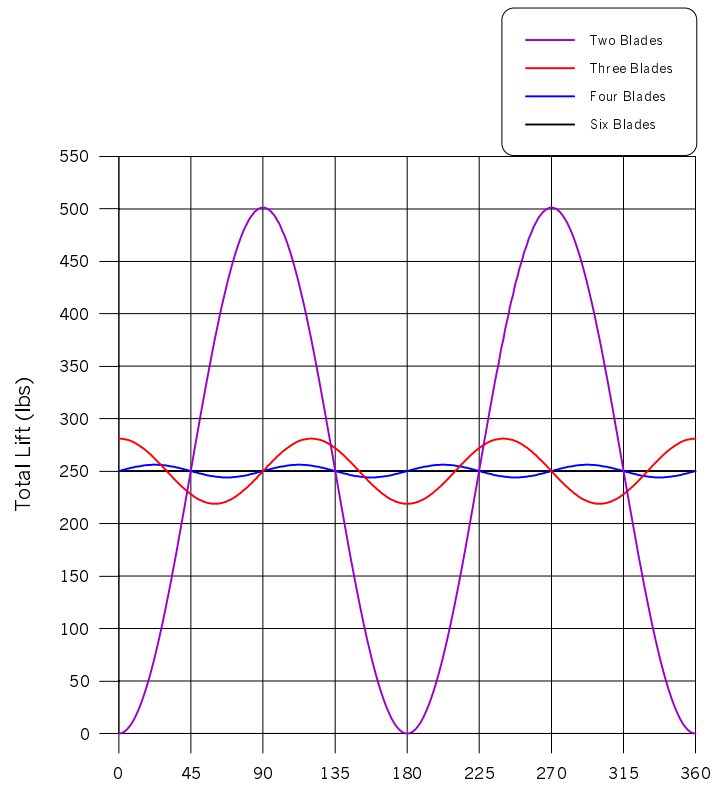


**Figure 4. Effect of the number of blades.**

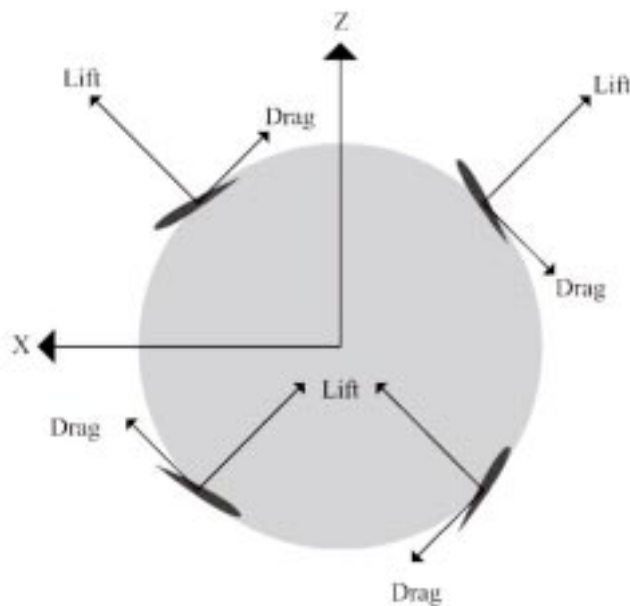


Figure 5. Lift and Drag

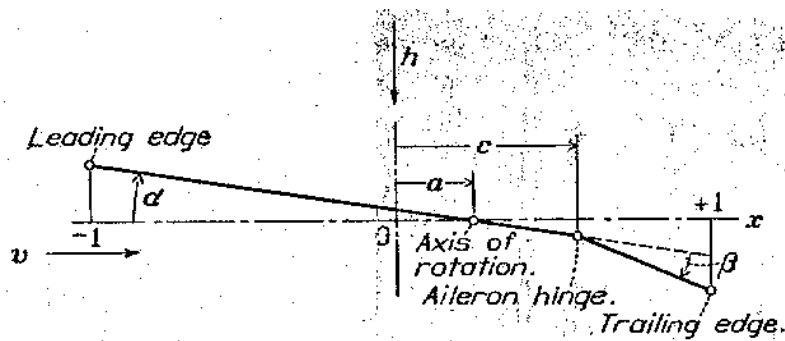


Figure 6. Definition of variables in Unsteady Aerodynamics Equations

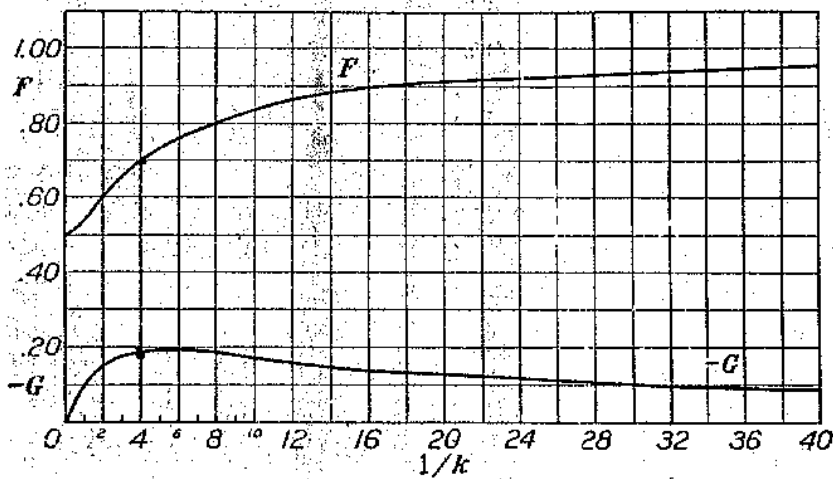
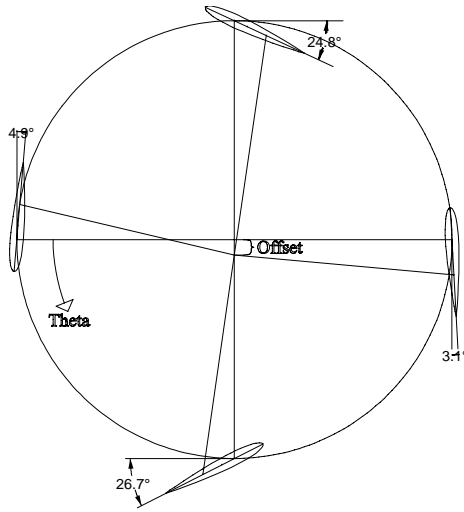
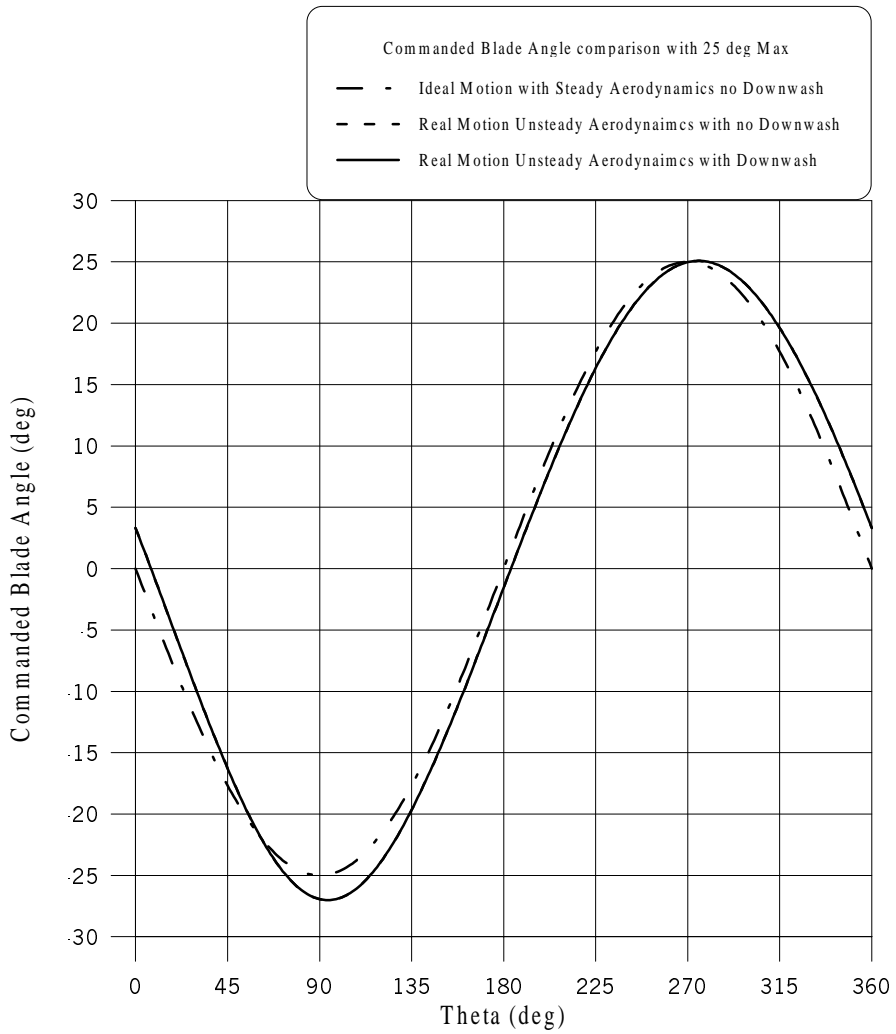


Figure 7. Plot of F and G



**Figure 8. Four-Bar Linkage Control Mechanism**



**Figure 9. Comparison of Ideal Motion and Real Motion**

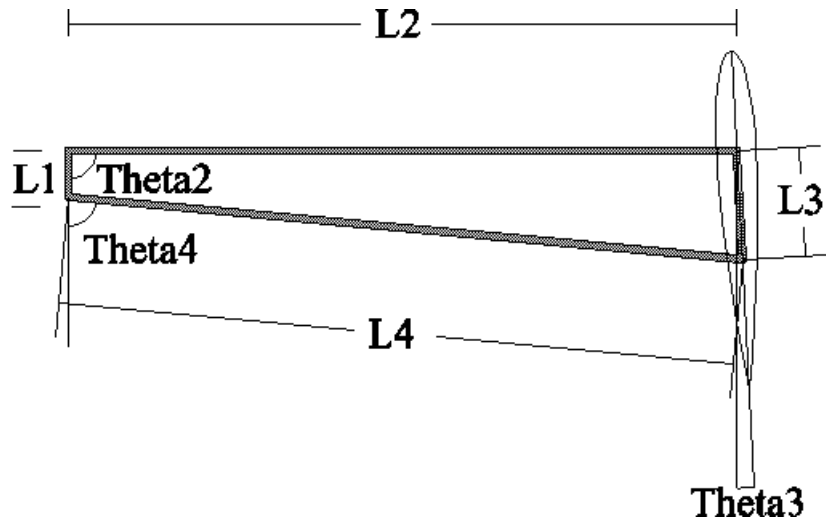


Figure 10. Typical Four-Bar System

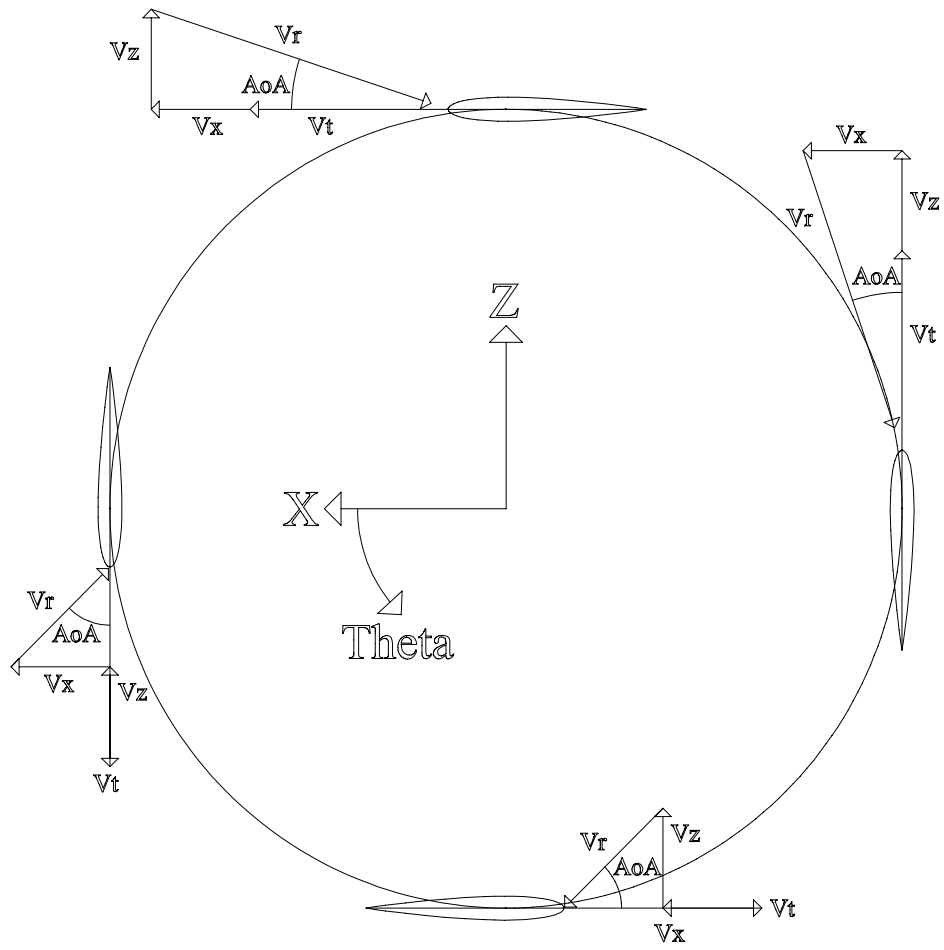
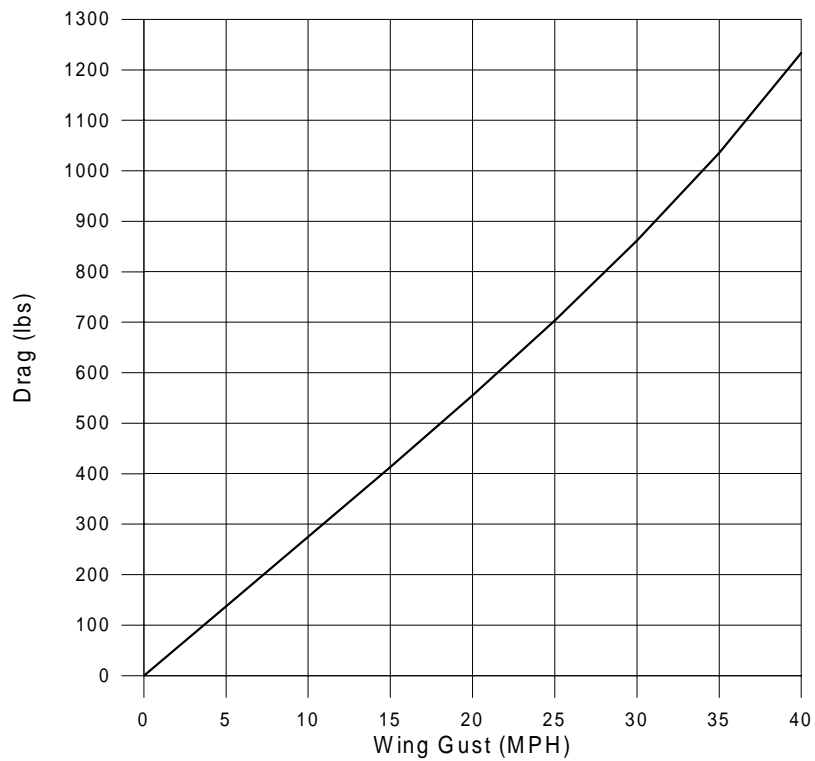
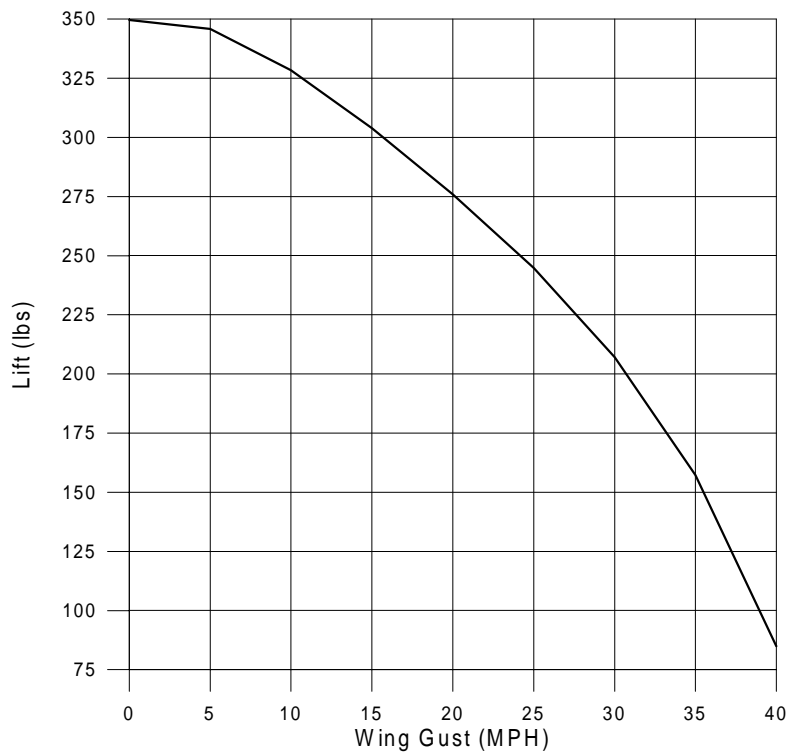


Figure 11. Definition of Propeller Motion



**Figure 12. Retarding Force/Drag due to Gust**



**Figure 13. Increase in lift due to Gust**

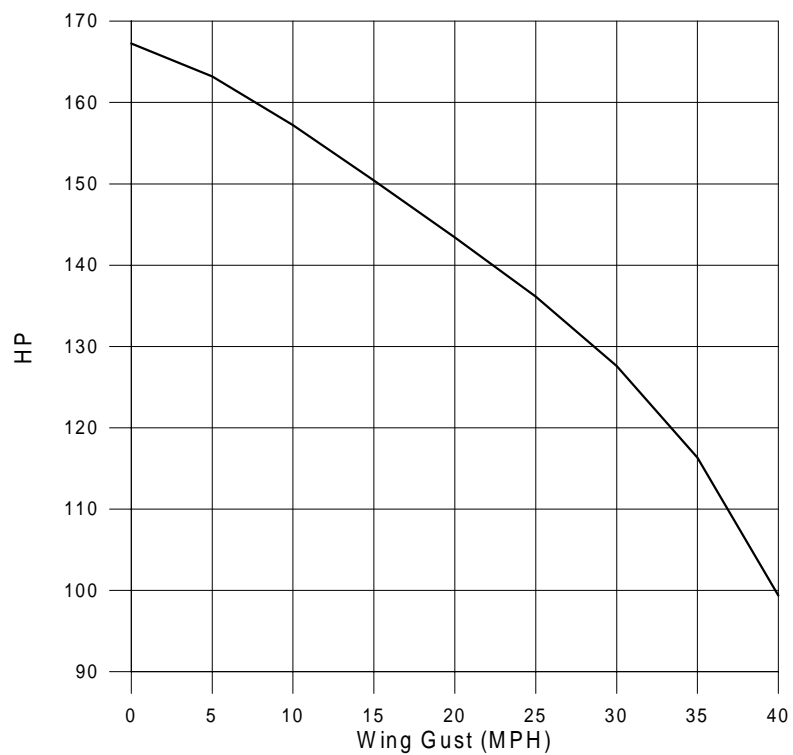


**Figure 14. Increase in HP due to Gust**

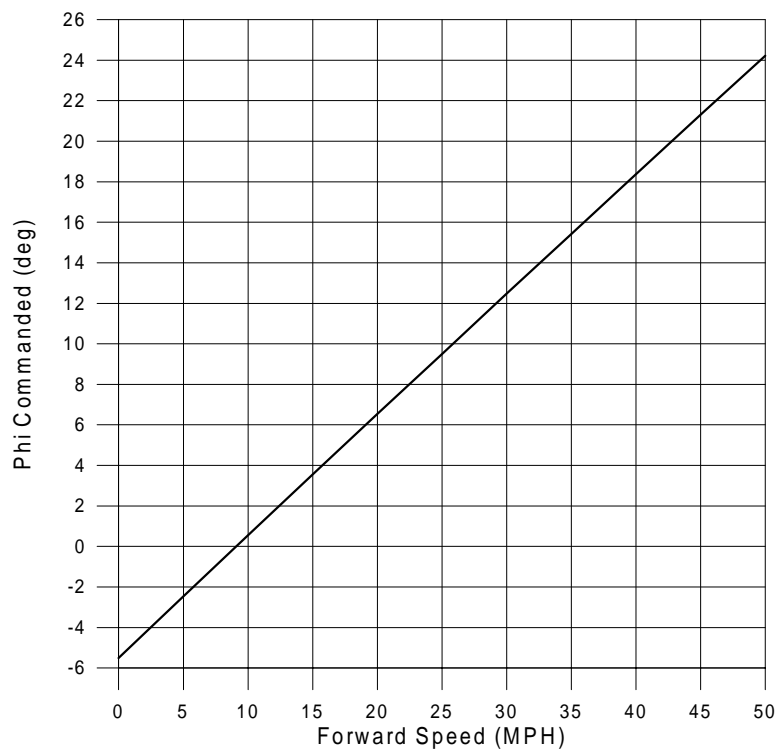


**Figure 15. Commanded Phi needed for Forward Flight**

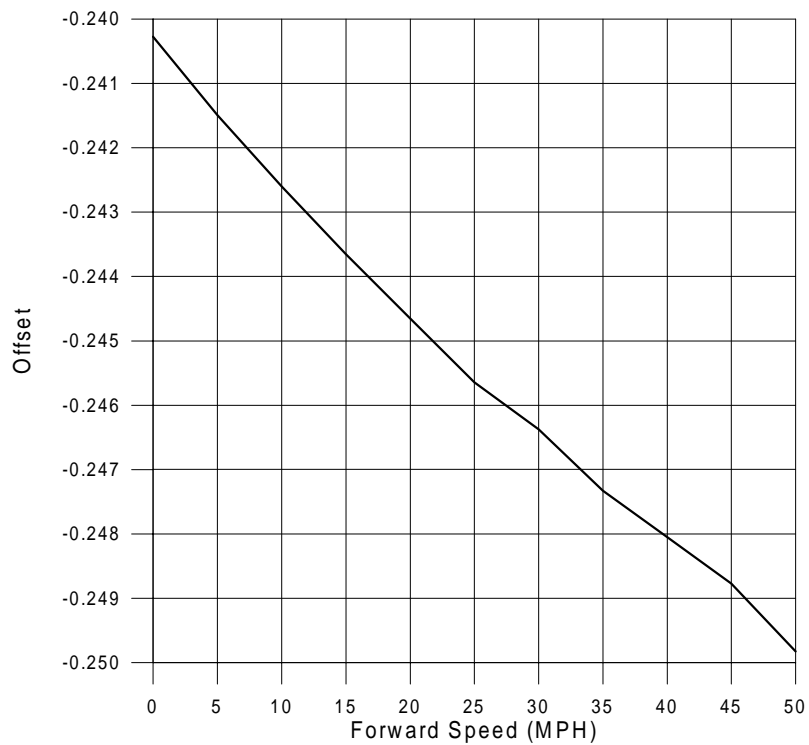


**Figure 16. Offset Required for Different Forward Speeds**

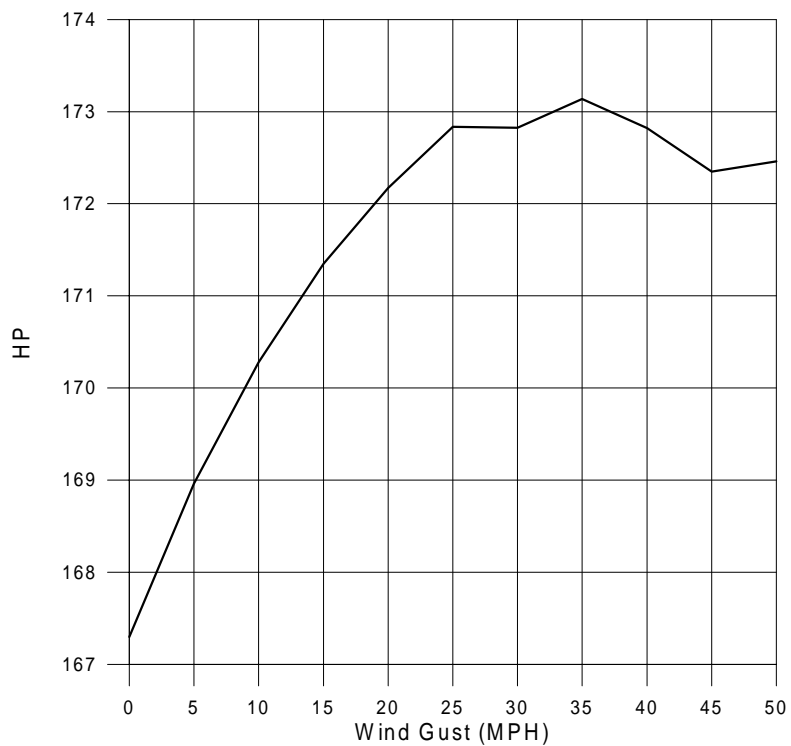


**Figure 17 HP required for Different Forward Speeds**

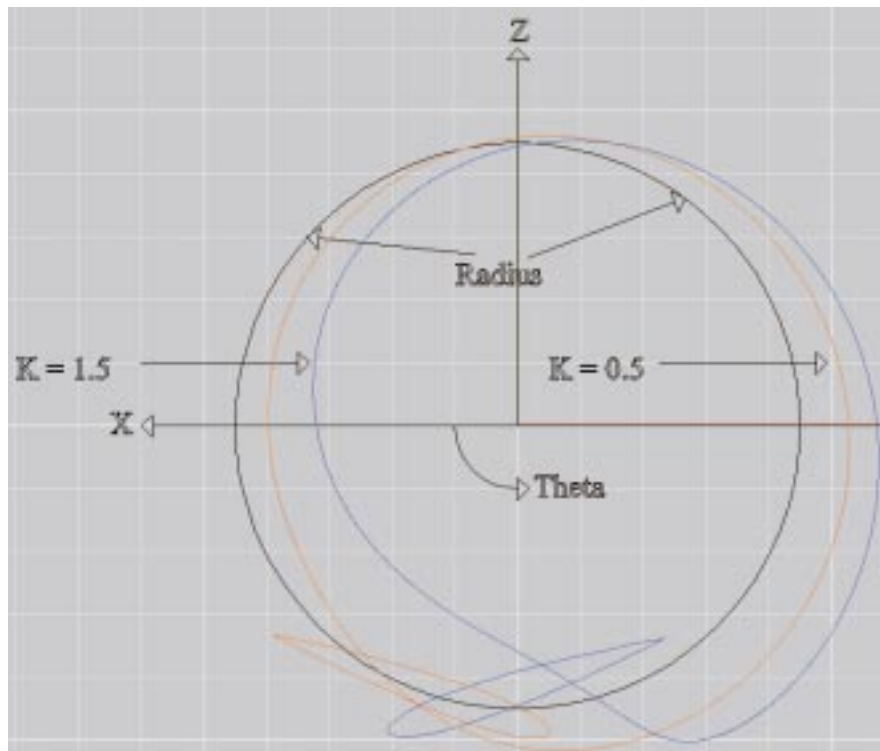


Figure 18. Cam Shape Needed for Advance Ratios Equal to 0.5 and 1.5

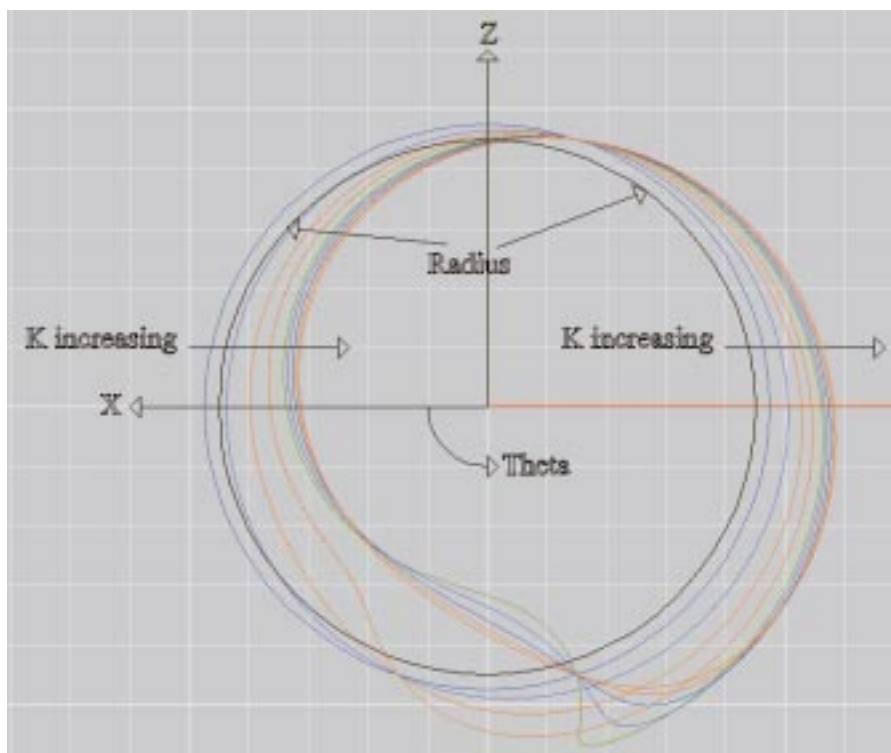


Figure 19. Cam Shape Needed for All Advance Ratios Between 0.0 and 2.0

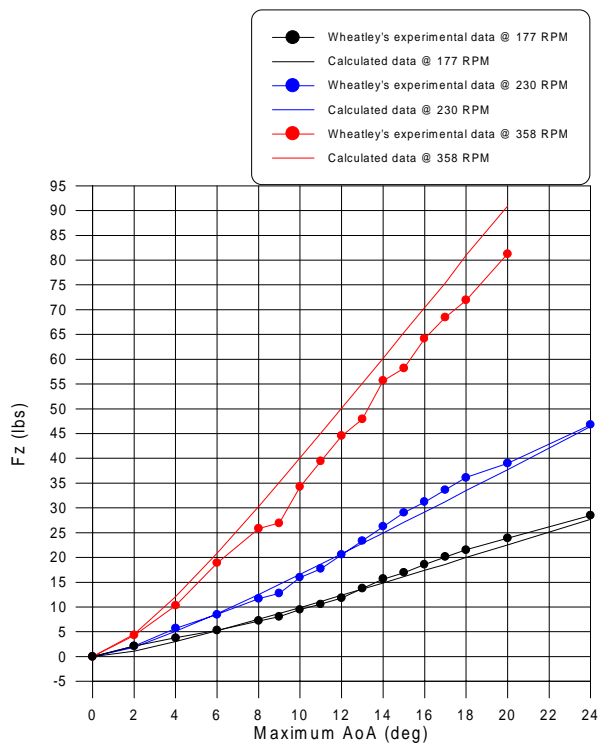


Figure 20 Comparison to Wheatley’s Wind Tunnel Data for Force in Z Direction

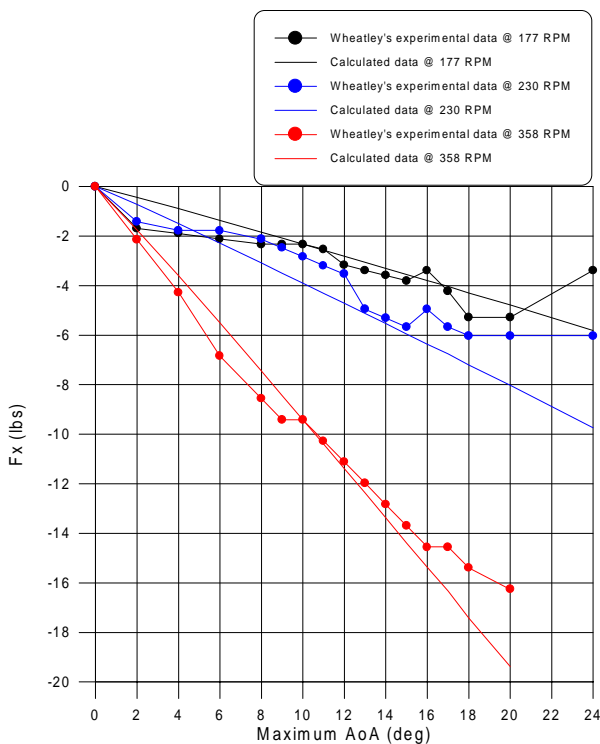


Figure 21 Comparison to Wheatley’s Wind Tunnel Data for Force in X Direction

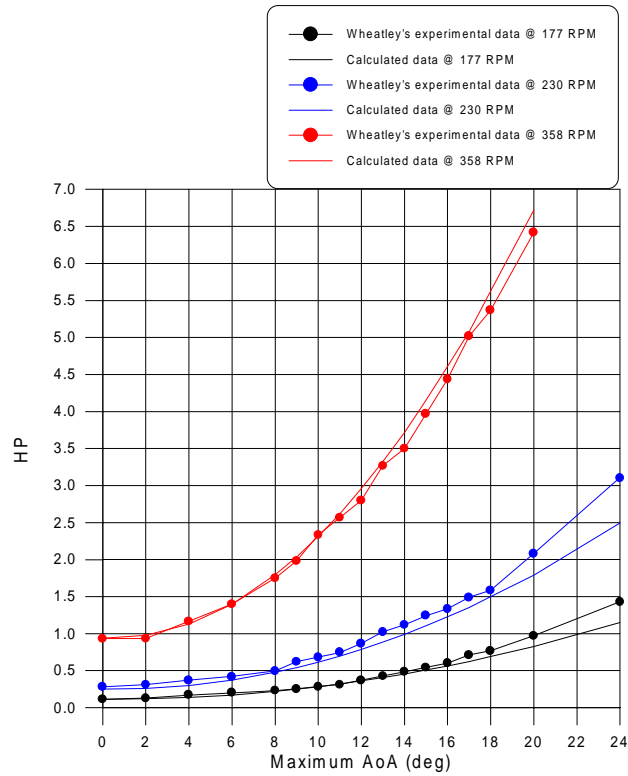


Figure 22 Comparison to Wheatley’s Wind Tunnel Data for Power

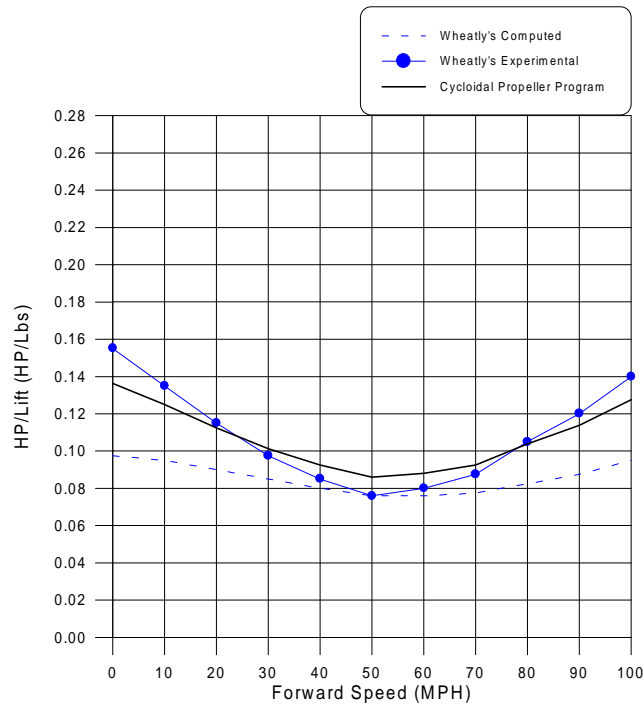
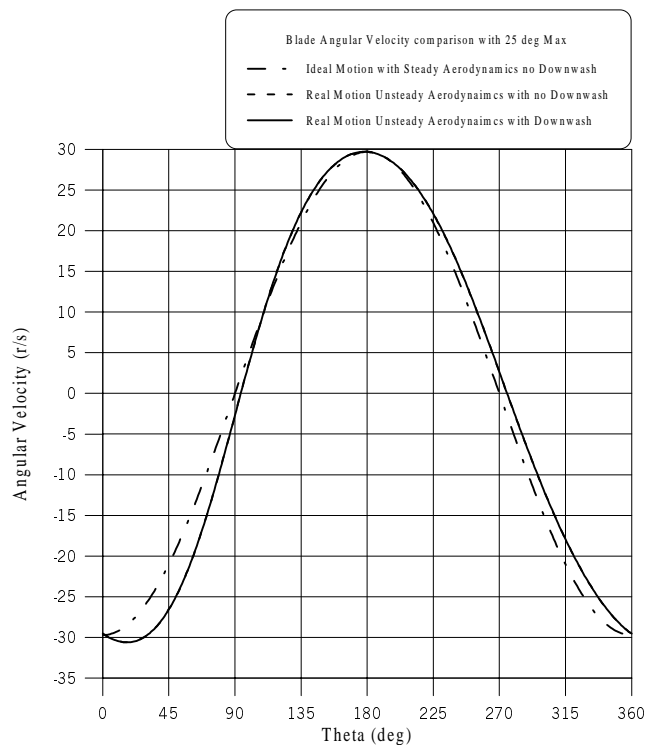
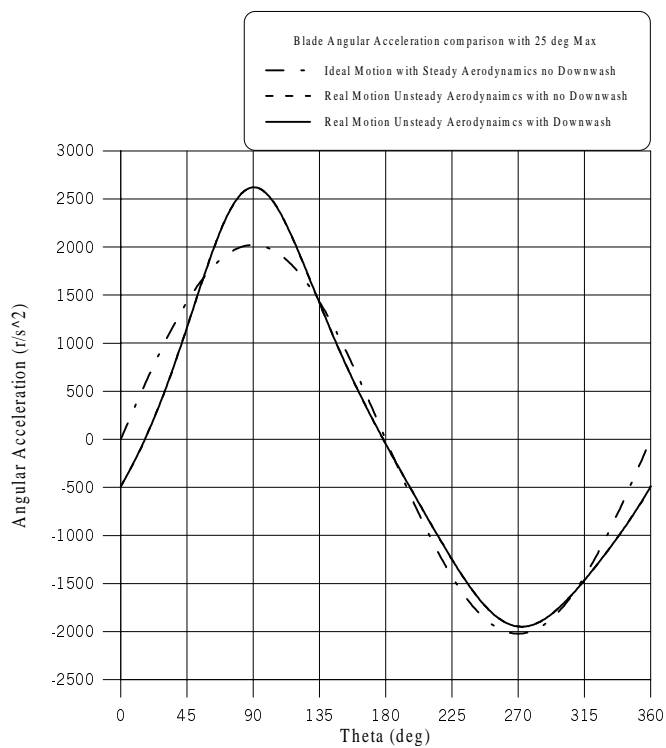


Figure 23 Comparing Wheatley’s and the Program’s Data for Different Forward Speeds



**Figure 24. Angular Velocity of the Blade**



**Figure 25. Angular Acceleration of the Blade**

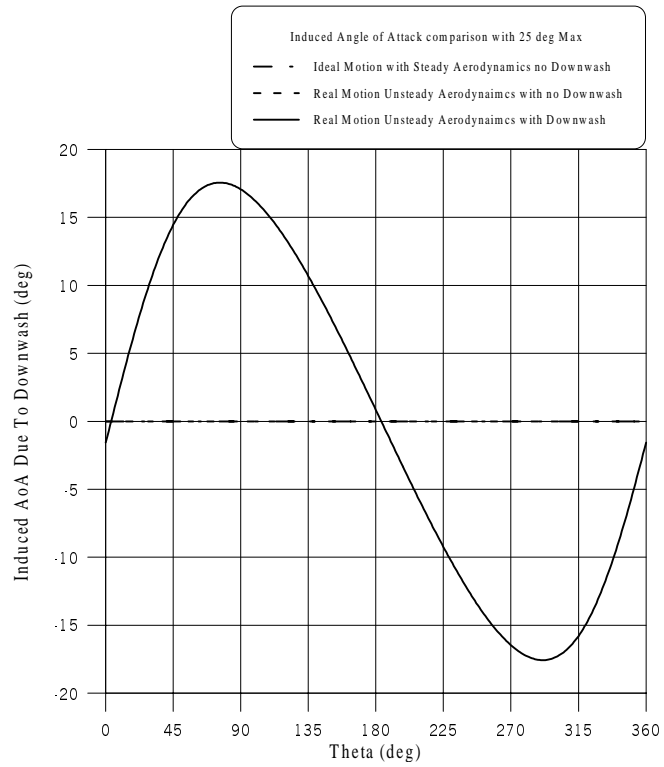


**Figure 26. Induced AoA caused by downwash**

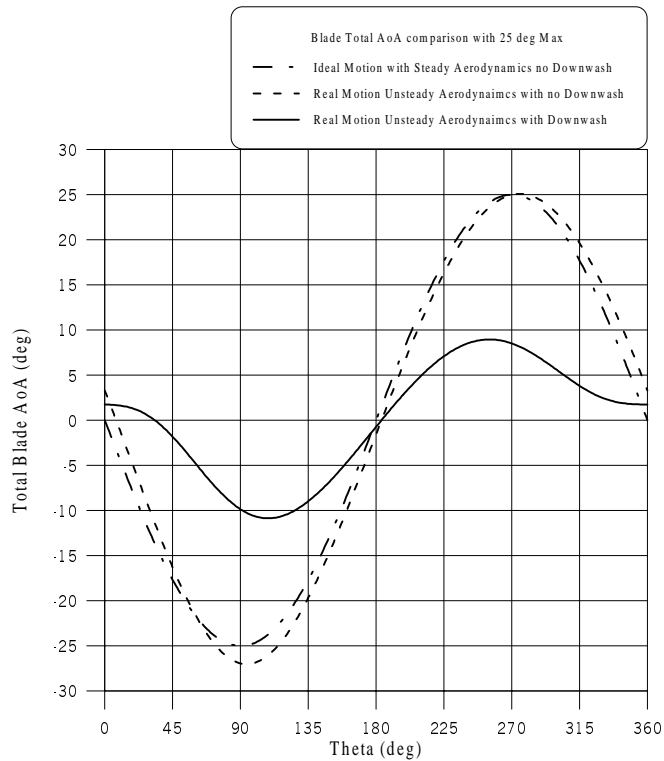


**Figure 27. Total AoA of the blade**

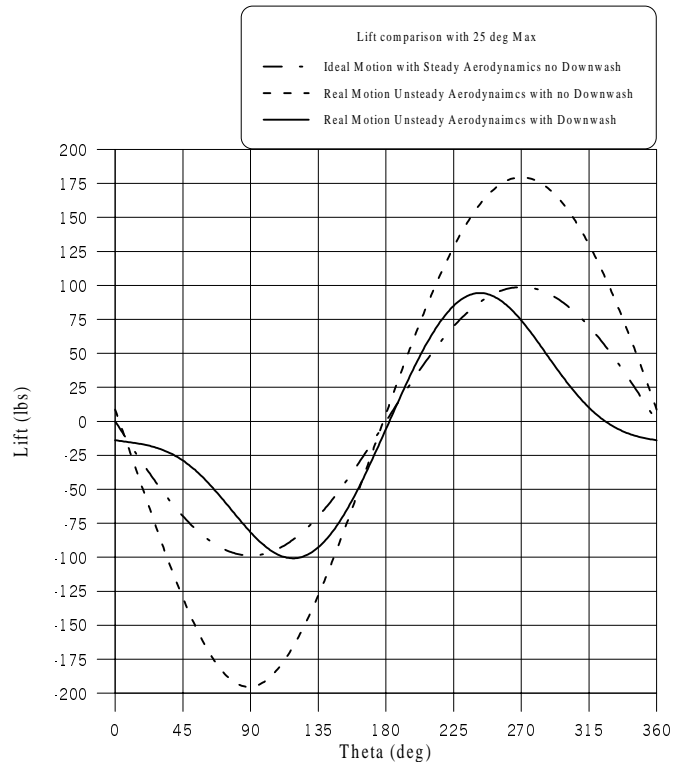


**Figure 28. Lift of the Blade**

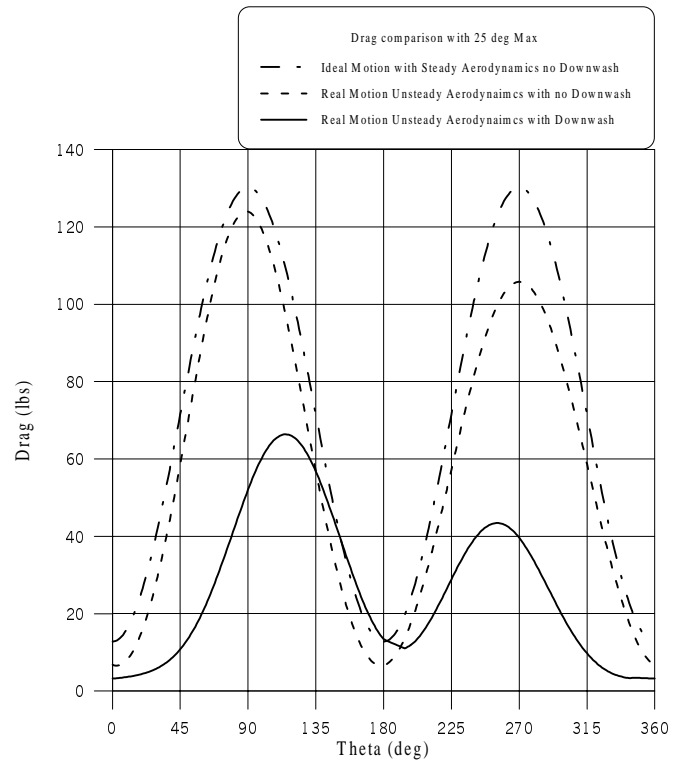


**Figure 29. Drag of the Blade**

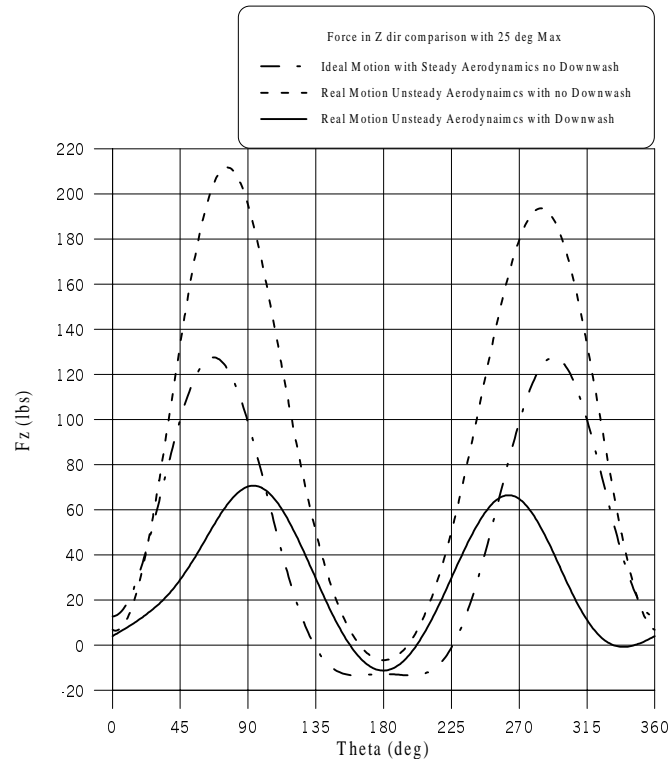


**Figure 30. Force in the Z direction produced by the blade**

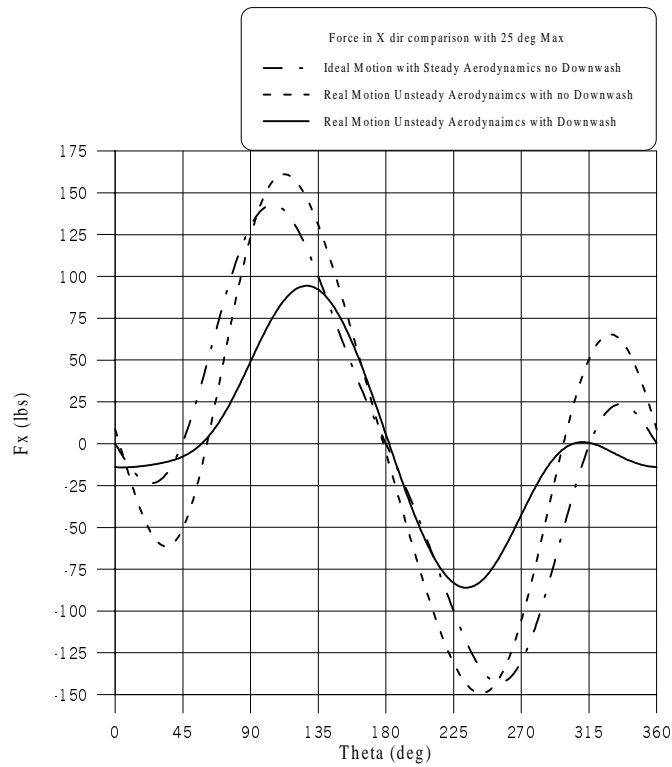


**Figure 31. Force in the X direction produced by the blade**

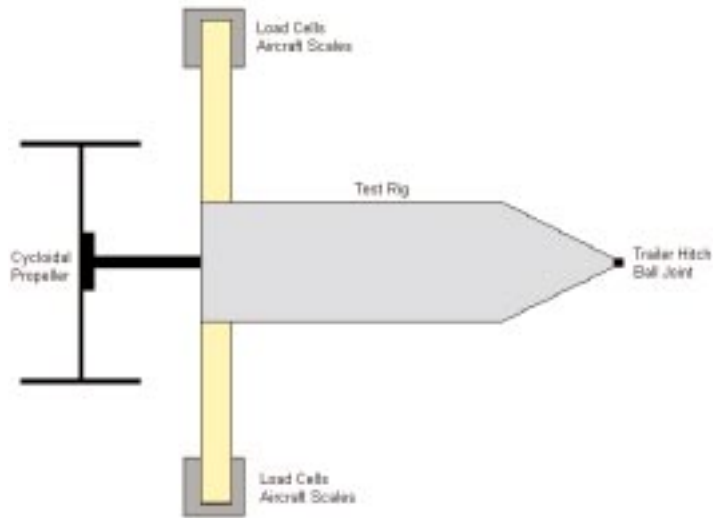


Figure 32. Sketch of Test Rig

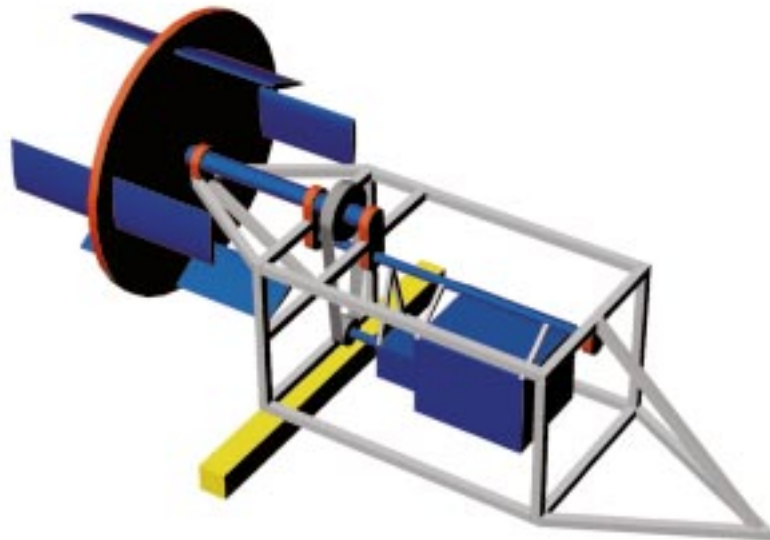


Figure 33. 3D View of Test Rig

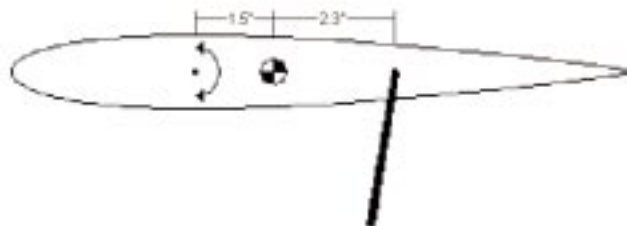


Figure 34. Blade Measurements Used in Bosch Cycloidal Propeller

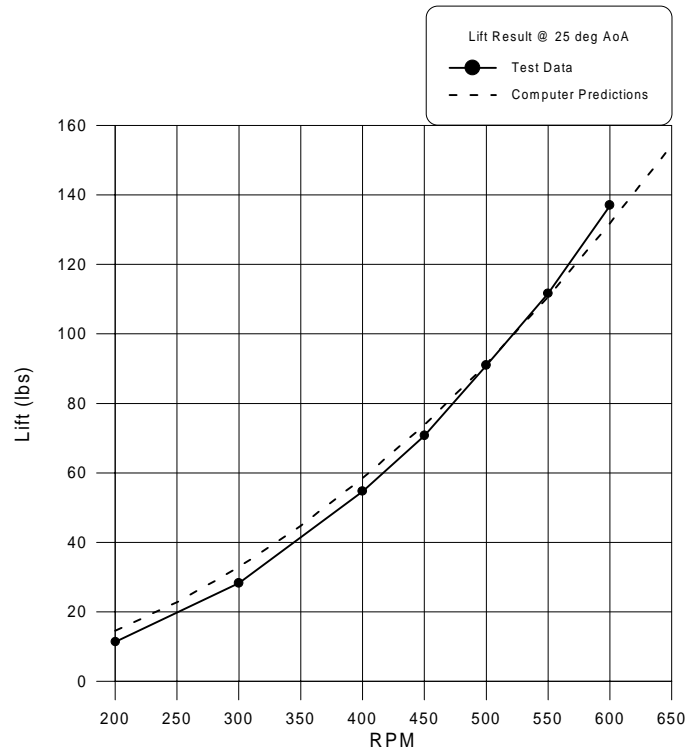


Figure 35. Lift Generated by Cycloidal Propeller Compared to Computer Predictions

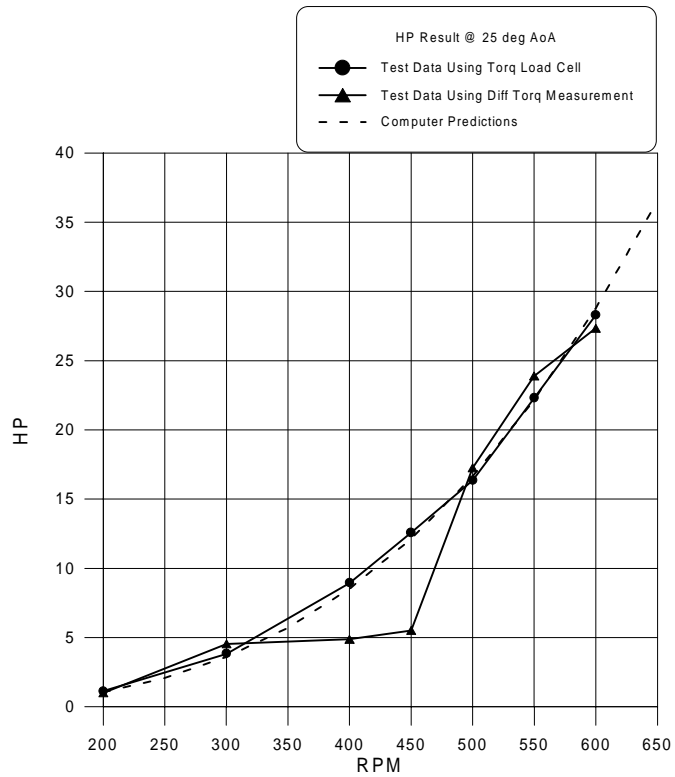


Figure 36. HP Required by Cycloidal Propeller Compared to Computer Predictions

APPENDIX B  
MATHCAD PROGRAM

Cycloidal propeller program by integration for ideal motion with steady aerodynamics

$$\text{RPM} := \frac{\pi \cdot \text{rad}}{30 \cdot \text{sec}}$$

Enter all of the blade data

Radius of the propeller	Full span of the blades	Chord of the blades	Number of blades
R := 2-ft	Span := 4-ft	C := 1-ft	numbld := 6

Oswald efficiency of the blades	2-D lift curve slope of NACA 0012	Parasite drag coefficient of NACA 0012
e := 0.4	C <sub>La2D</sub> := 6.0161	C <sub>D0</sub> := 0.05

Enter other data about the cycloidal propeller

$\Omega := 650 \text{RPM}$	$\Omega = 68.068 \frac{\text{rad}}{\text{sec}}$	Speed of the propeller
----------------------------	---	------------------------

$V_r := R \cdot \Omega$	$V_r = 136.136 \frac{\text{ft}}{\text{sec}}$	Speed of the air at the blades
-------------------------	--	--------------------------------

$\beta_{\text{Max}} := 20 \text{deg}$	Maximum commanded angle of attack
---------------------------------------	-----------------------------------

$\rho := 0.0023769 \frac{\text{lb} \cdot \text{sec}^2}{\text{ft}^4}$	Density of air at sea level
--	-----------------------------

$\phi := 0.0 \text{deg}$	Rotation of the lift vector
--------------------------	-----------------------------

Start with some different theta's between 0 and 360 degrees

$\theta := 0 \text{deg}, 1 \text{deg} \dots 360 \text{deg}$

Begin calculations

$S := \text{Span} \cdot C$	$S = 4 \text{ft}^2$	Area of one blade
----------------------------	---------------------	-------------------

$AR := \frac{\text{Span}^2}{S}$	$AR = 4$	Aspect ratio of the blade
---------------------------------	----------	---------------------------

$C_{La3D} := \frac{2 \cdot \pi \cdot AR}{2 + \sqrt{\left(\frac{AR \cdot 2 \cdot \pi}{C_{La2D}}\right)^2 + 4}}$	$C_{La3D} = 3.79$	3 D lift curve slope of the blade
--	-------------------	-----------------------------------

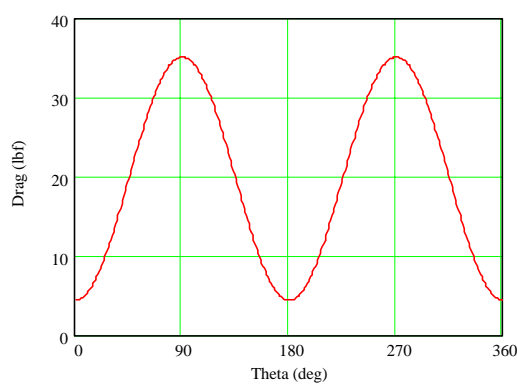
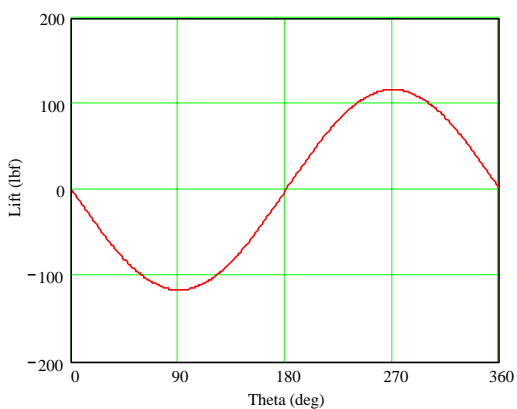
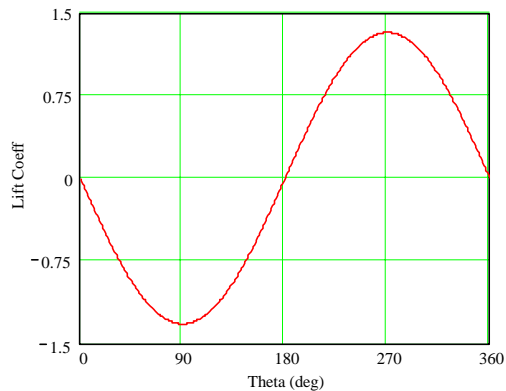
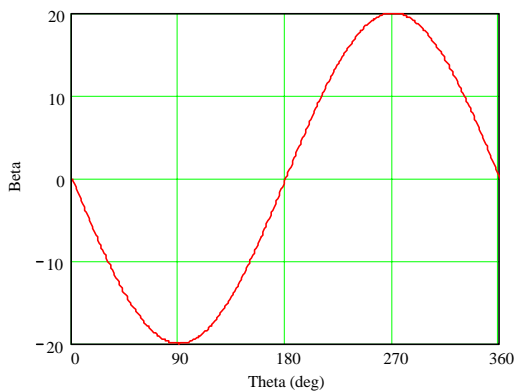
$\beta(\theta) := -\beta_{\text{Max}} \cdot \sin(\theta - \phi)$	Commanded blade angle
--	-----------------------

$C_L(\theta) := C_{La3D} \cdot \beta(\theta)$	Lift coefficient
---	------------------

$\text{Lif}(\theta) := \frac{1}{2} \cdot \rho \cdot V_r^2 \cdot S \cdot C_L(\theta)$	Lift for that blade
--	---------------------

$C_D(\theta) := C_{D0} + \frac{C_L(\theta)^2}{\pi \cdot AR \cdot e}$	Drag coefficient
--	------------------

$\text{Drag}(\theta) := \frac{1}{2} \cdot \rho \cdot V_r^2 \cdot S \cdot C_D(\theta)$	Drag for that blade
---	---------------------

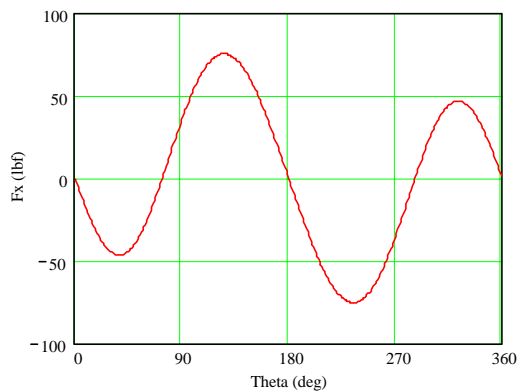
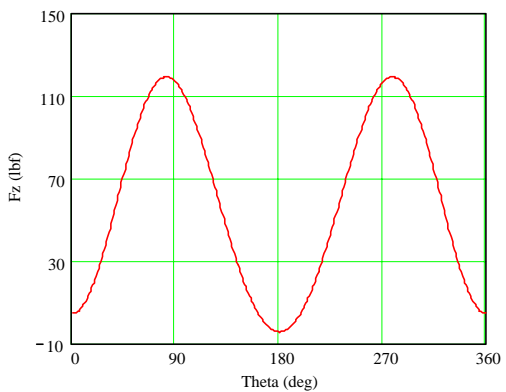


Force in the Z direction

$$F_Z(\theta) := -Lift(\theta) \cdot \sin(\theta) + Drag(\theta) \cdot \cos(\theta)$$

Force in the X direction

$$F_X(\theta) := Lift(\theta) \cdot \cos(\theta) + Drag(\theta) \cdot \sin(\theta)$$



Calculate the average lift for one blade,

$$Ave := \frac{\int_0^{360} F_Z(\theta) d\theta}{360}$$

Ave = 58.287lbf

Calculate the total lift generated by a propeller with X blades

Total\_Lift := Ave · numblld      Total\_Lift = 349.722lbf

## APPENDIX C

### REAL MOTION UNSTEADY AERODYNAMICS PROGRAM













```
+      Alpha(K,1)*180.0/Pi, (Omega3(K,1)-Omega),  
+      Omega4(K,1), Acc3(K,1), Acc4(K,1)  
55  Format (f5.1,2x,f6.2,2x,f7.2,2x,f7.2,2x,f6.2,2x,f7.2,2x,f6.2,2x,  
+      f8.2,2x,f8.2)  
60  Continue  
End
```